

# DIRECT FREQUENCY COMB SPECTROSCOPY

MATTHEW C. STOWE<sup>1</sup>, MICHAEL J. THORPE<sup>1</sup>, AVI PE'ER<sup>1</sup>, JUN YE<sup>1</sup>,  
JASON E. STALNAKER<sup>2</sup>, VLADISLAV GERGINOV<sup>2</sup> and SCOTT A. DIDDAMS<sup>2</sup>

<sup>1</sup>JILA, National Institute of Standards and Technology and University of Colorado,  
Department of Physics, University of Colorado, Boulder, Colorado 80309-0440, USA

<sup>2</sup>Time and Frequency Division, National Institute of Standards and Technology,  
Boulder, Colorado 80305, USA

1. Introduction and Historical Background . . . . .	2
2. Comb Control and Detection . . . . .	5
2.1. Comb Degrees of Freedom . . . . .	5
2.2. Control of Comb via an Optical Cavity . . . . .	8
3. Direct Frequency Comb Spectroscopy . . . . .	12
3.1. Theoretical Treatments . . . . .	13
3.2. Single-Photon DFCS . . . . .	15
3.3. Multi-Photon DFCS . . . . .	22
3.4. Short Wavelength DFCS . . . . .	29
4. Multi-Frequency Parallel Spectroscopy . . . . .	30
4.1. Cavity Enhanced DFCS . . . . .	32
5. Coherent Control Applications . . . . .	38
5.1. High Resolution Coherent Control . . . . .	39
5.2. Extension of DFCS to Strong Field Coherent Control . . . . .	40
6. Future Outlook . . . . .	45
6.1. Atomic Clock Applications . . . . .	45
6.2. XUV Comb Development . . . . .	46
6.3. Future VUV Comb Spectroscopy . . . . .	49
6.4. Optical Frequency Synthesis and Waveform Generation . . . . .	51
7. Concluding Remarks . . . . .	52
8. Acknowledgements . . . . .	52
9. References . . . . .	53

## Abstract

Besides serving as a frequency counter or clockwork, an optical frequency comb can be used directly for spectroscopy, thus the name Direct Frequency Comb Spectroscopy (DFCS). Precise phase coherence among successive ultrashort pulses allow one to explore both fast dynamics in the time domain and high-resolution structural information in the frequency domain. Coherent accumulation of weak pulses can lead to strong field effects. Combined with spectral manipulation, high-resolution quantum control can be implemented. The large number of frequency comb components also provide a massive set of parallel detection channels to gather spec-

troscopic information. In this chapter we provide a detailed review of some of the current applications that exploit these unique features, and discuss several future directions of DFCS.

## 1. Introduction and Historical Background

At the end of the 1990s the mode-locked femtosecond laser and its associated optical frequency comb made an unanticipated entry into the field of precision optical frequency metrology (Udem et al., 1999a, 1999b; Diddams et al., 2000; Jones et al., 2000). It is difficult to overstate the impact of this new technology on frequency metrology research (Hall, 2006; Hänsch, 2006). In simple terms, the femtosecond laser frequency comb transformed optical frequency standards into optical clocks by providing a straightforward means to count optical cycles (Diddams et al., 2001; Ye et al., 2001). Just as important, a stabilized frequency comb permits the easy comparison of optical standards separated by hundreds of terahertz (Diddams et al., 2001; Stenger et al., 2002), offers new tools for frequency transfer (Holman et al., 2004; Foreman et al., 2007), introduces new approaches to length metrology (Ye, 2004; Minoshima and Matsumoto, 2000), and provides the carrier-envelope control required for phase-sensitive nonlinear optics and attosecond physics (Paulus et al., 2001; Baltuška et al., 2003).

Beyond its enabling advances in optical frequency metrology, a stabilized optical frequency comb can also be a versatile spectroscopic tool, providing excellent accuracy, high spectral purity, and at the same time broad spectral coverage. In fact, the concept of using the frequency comb from a mode-locked laser for high resolution spectroscopy precedes the more recent comb-related excitement by several decades. The 1970s saw the emergence of the theory and experiments containing the roots of the ideas that will be discussed in detail in this review. While the pulses were longer (nano- or picosecond compared with femtosecond) and the frequency control was rudimentary by today's standards, many of the early experiments already highlighted the advantages of a mode-locked laser frequency comb for multi-photon spectroscopy and measuring optical frequency differences.

Considering our present-day understanding of the frequency comb, it is not surprising that these early experiments emerged as either time- or frequency-domain interpretations of the interaction of a series of coherent pulses with an atomic system. From the time-domain perspective, two early experiments were cast as variations of Ramsey spectroscopy applied to two-photon transitions (Salour and Cohen-Tannoudji, 1977; Teets et al., 1977). In both cases, linewidths less than the pulse bandwidth were observed due to the coherence

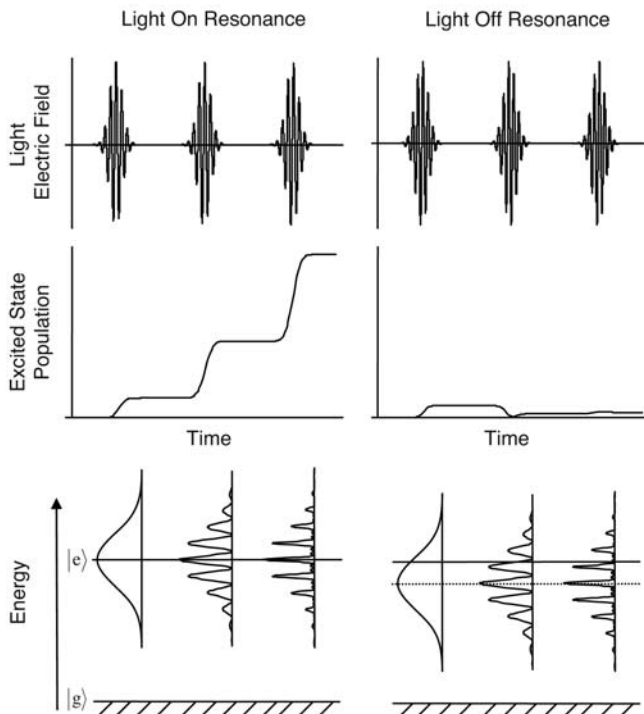


FIG. 1. Time- and frequency-domain interpretations of the interaction of a series of short pulses with an atomic system. The bandwidth of the pulse is much broader than the linewidth of the resonance. When the light is on resonance, the contribution to the atomic polarization adds constructively from pulse to pulse, and population accumulates in the excited state (left column). In the frequency domain, this corresponds to one of the comb modes being on resonance with the transition as shown in the lower left frame. Note that the frequency comb is not defined for a single pulse, but builds up from the interference of several pulses, as shown in the lower plots. In the off resonance case, subsequent pulses arrive out of phase with the evolving polarization and population is moved back to the ground state (right column). This corresponds to the case of a comb mode not overlapping with the transition frequency.

between the temporally-separated pulses as illustrated in Fig. 1. Early experiments that approached spectroscopy from the frequency domain focused on the advantage the frequency comb brings to multi-photon transitions in which pairs of comb modes are summed or subtracted to match the atomic resonance. Two examples are shown in Fig. 2. The case of the lambda transition shown in Fig. 2(a) can be viewed as Raman spectroscopy in which multiple comb components contribute to the resonant transfer of population between the two ground states under the requirement that the difference in energy between the ground

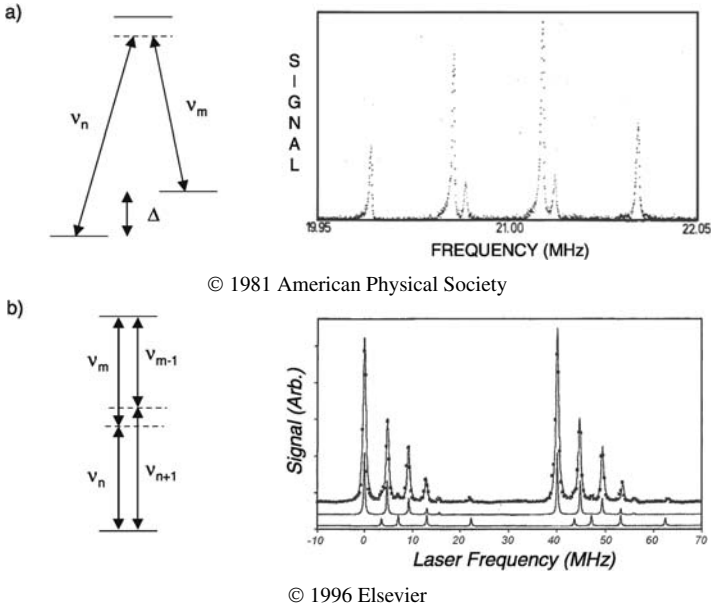


FIG. 2. Two-photon comb spectroscopy in (a) lambda and (b) ladder systems. In the lambda system resonances are observed when the difference in two comb mode frequencies (or an integer multiply thereof) matches the lower level splitting. An example from the work of Mlynek et al. (1981) is shown where the pulse repetition rate is varied. In this case, the six different resonances result from different hyperfine and magnetic sub-levels of the sodium  $D_1$  transition. In the case of the more conventional two-photon transition (b), an example from the work of Snadden et al. (1996) in Rb shows the resonances due to the hyperfine structure in the  $5S$ – $5D$  transition. Because of the periodic structure of the frequency comb, the data repeat every 40 MHz ( $1/2$  the comb spacing). [Figure (a) reprinted with permission from Mlynek et al. (1981). Figure (b) reprinted with permission from Snadden et al. (1996).]

states corresponds to a harmonic of the comb mode spacing (Mlynek et al., 1981; Fukuda et al., 1981; Harde and Burggraf, 1982). Related approaches have proved to be of interest in the area of coherent population trapping (Diddams et al., 1998; Brattke et al., 1998). In Fig. 2(b) one sees the classic two-photon transition in which multiple pairs of comb modes sum together to reach the excited state (Eckstein et al., 1978; Baklanov and Chebotayev, 1977; Hänsch and Wong, 1980; Snadden et al., 1996). This basic approach has been extended to experiments in saturated absorption and polarization spectroscopy (Couillaud et al., 1980; Ferguson et al., 1979). In contrast to the case of the lambda transition, this spectroscopy is sensitive not only to the mode spacing but also the absolute frequency of the comb modes—a point that we will return to later.

## 2. Comb Control and Detection

In this section we provide a brief review of optical frequency comb structure and the means for its stabilization. More detailed reviews can be found in [Cundiff et al. \(2001\)](#), [Cundiff and Ye \(2003\)](#), [Ye et al. \(2003\)](#), [Ye and Cundiff \(2005\)](#). Passive optical cavities will also be discussed here, which will serve three roles: frequency comb stabilization; buildup of intracavity field strength; and enhancement of spectroscopic detection sensitivity.

### 2.1. COMB DEGREES OF FREEDOM

The frequency spectrum of an ideal mode-locked laser is generally composed of hundreds of thousands of equidistant modes spaced by the repetition rate of the laser, thus the name optical frequency comb. In practice, however, a mode-locked laser exhibits noise on the optical phase and repetition rate of the emitted pulses. In this section we briefly review the relevant degrees of freedom governing the laser frequency spectrum and the common methods of stabilization.

There are only two degrees of freedom necessary to uniquely specify the frequency of every comb mode ([Reichert et al., 1999](#)). The first is the repetition rate of the laser,  $f_r$ , defined as the inverse of the inter-pulse period. As can be seen in [Fig. 3](#) the comb mode spacing is exactly  $f_r$ . Secondly, the rate change of optical phase from pulse to pulse must be specified. Referring to [Fig. 3](#) the carrier-envelope offset phase,  $\phi_{ce}$ , is defined as the relative phase between the peak of the pulse envelope and the underlying electric field. In general the  $\phi_{ce}$  changes between pulses, it is this change,  $\Delta\phi_{ce}$ , which determines the offset frequency,  $f_o$ , of the comb modes as shown in [Fig. 3](#). Using these definitions the frequency of the mode indexed by  $n$  is given by  $\nu_n = nf_r + f_o$ , with  $f_o = f_r \frac{\Delta\phi_{ce}}{2\pi}$ . For a laser with a repetition rate between 1 to 100 MHz and center wavelength of 800 nm the mode index  $n$  is of order  $10^5$  to  $10^6$ . In general,  $f_r$  and  $f_o$  can be independently measured and then controlled via two servo transducers acting on the cavity length and the dispersion of the mode-locked laser.

The laser repetition rate  $f_r$  is generally directly measured on a fast, multi-GHz bandwidth, photodiode. This produces a series of radio frequency (RF) beats at multiples of  $f_r$  which can be used for phase locking to an RF reference such as a crystal oscillator with low short-term noise. To achieve superior phase sensitivity, one of the high harmonics of  $f_r$  is used for the phase lock, for example the tenth harmonic of a 100 MHz repetition rate laser can be locked to a 1 GHz reference oscillator. The beat phase between the measured  $f_r$  harmonic and the reference is filtered and amplified for use as an error signal to servo the laser cavity length via a piezo-electric transducer (PZT) mounted output coupler. Because an optical frequency is related to the repetition rate by the mode number, any noise on

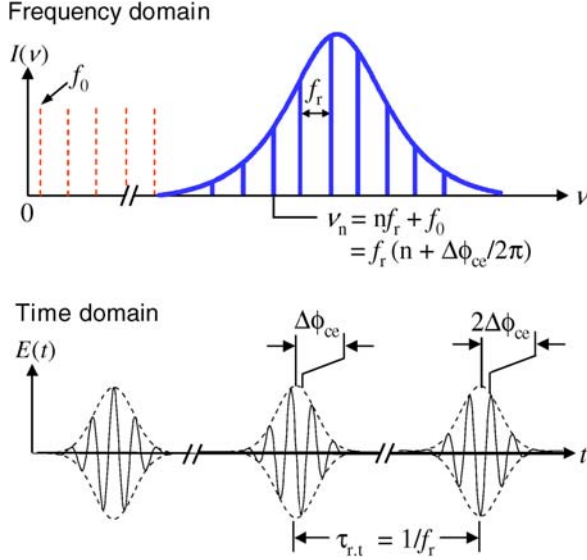


FIG. 3. (Top panel) Frequency-domain picture of the femtosecond pulse train indicating the comb modes under a Gaussian spectral envelope. The modes are equally spaced by  $f_r$  and offset from exact  $f_r$  harmonics by  $f_0$ . The expression for the frequency of the  $n$ th mode is given. (Bottom panel) Time-domain picture of the corresponding infinite periodic pulse train. Note that  $\phi_{ce}$  of the first pulse is zero then evolves to a nonzero value by the second pulse, thus  $\Delta\phi_{ce} \neq 0$  so  $f_0 \neq 0$ .

the repetition rate is multiplied by  $10^5$ – $10^6$  for typical mode numbers. Thus, the short term stability of the reference oscillator plays a crucial role in the resulting comb mode linewidth. With some of the best available RF sources one can obtain fractional instabilities on the order of  $10^{-13}$  in one second. In fact, the ultimate performance in frequency comb stabilization is via an optical approach: direct comparisons between frequency comb modes against optical references such as a single frequency continuous-wave (cw) laser (Diddams et al., 2000; Ye et al., 2000, 2001) or a high-finesse optical cavity (Jones and Diels, 2001; Jones et al., 2004). The direct optical approach permits the transfer of superior stability optical standards to the frequency comb, yielding comb instabilities of order  $10^{-15}$  in one second and Hz-level linewidths (Bartels et al., 2004a; Ludlow et al., 2006).

Direct detection and stabilization of the offset frequency,  $f_0$ , is somewhat more complicated than  $f_r$ . The typical approach for measuring  $f_0$  (Reichert et al., 1999; Telle et al., 1999) requires an octave spanning pulse bandwidth. If the pulse bandwidth spans one octave then it contains two frequencies,  $\nu_1 = n_1 f_r + f_0$  and  $\nu_2 = n_2 f_r + f_0$ , where  $n_2 = 2n_1$ . The second harmonic of  $\nu_1$  is  $2\nu_1 = 2n_1 f_r + 2f_0$ , which upon forming a heterodyne beat with  $\nu_2$  yields

a beat note at the desired  $f_o$  frequency. This technique is referred to as self-referencing because it forms the beat note entirely from the laser output without any separate reference frequencies. It is now also possible to obtain an octave bandwidth directly from a suitably constructed Ti:sapphire laser (Ell et al., 2001; Fortier et al., 2006a, 2003; Mücke et al., 2005). A common technique for generating the required bandwidth is via four-wave mixing in an extra-cavity highly nonlinear fiber. Other techniques for measuring  $f_o$  require less than an octave of bandwidth. For example, one needs only  $2/3$  of an octave bandwidth by using a heterodyne beat between two sets of adjacent modes, one formed by doubling the high-frequency portion of the original comb spectrum and the other from tripling the low-frequency portion (Telle et al., 1999; Ramond et al., 2002).

It was the development of dispersion modified micro-structured fiber (Ranka et al., 2000; Dudley et al., 2006) that enabled the first experimental demonstration of self-referencing (Jones et al., 2000; Apolonski et al., 2000). Micro-structure fiber, also called photonic crystal fiber, exhibits two important features for efficiently producing an octave spanning bandwidth. Micro-structure fiber gets its name from the regular pattern of air holes that extend the length of the fiber and surrounding the core, forming a photonic band gap to confine the light. By tuning the waveguide dispersion of the fiber the net dispersion can be made zero near the desired input pulse wavelength. Typically such a fiber has a core diameter of about  $1.7 \mu\text{m}$  for a zero dispersion point at  $800 \text{ nm}$ . Confining the pulse to such a small area can generate extremely large peak intensities, which due to the zero dispersion property may persist through the fiber with minimal pulse stretching. This combination of high intensity over a long interaction length allows for efficient four-wave mixing. In practice transform limited pulses with energies of order nanojoules can be used with approximately  $10 \text{ cm}$  of fiber to generate the necessary octave bandwidth.

To understand how to servo the laser and thus control  $f_o$  we must first understand the origin of the phase,  $\phi_{ce}$ . Recall that  $\phi_{ce}$  is defined between the pulse envelope, which travels at the group velocity  $v_g$ , and the underlying electric field, which travels at the phase velocity  $v_p$ . In the laser cavity the difference of  $v_g$  and  $v_p$  results in a generally nonzero  $\Delta\phi_{ce}$  given by

$$\Delta\phi_{ce} = l_c \omega_c \left( \frac{1}{v_g} - \frac{1}{v_p} \right),$$

where  $l_c$  is the cavity round trip length and  $\omega_c$  is the carrier frequency. With this knowledge in mind it is clear that tuning the dispersion of the cavity will also change  $f_o$ . This was first accomplished by tilting the end mirror of a linear cavity in which the spectrum is spatially dispersed via the intracavity prisms, the resulting wavelength-dependent extra path length changes the group velocity. Experimentally this can be done by mounting the end mirror

after the intracavity prism pair on a split PZT that is driven such that the mirror tilts in response to the error signal (Reichert et al., 1999; Cundiff et al., 2001). Alternatively, one can change the dispersion of the laser cavity via control of the pump power (Holman et al., 2003a). This approach can achieve a typical servo bandwidth of the order of 100 kHz. Once  $f_o$  is stabilized,  $f_r$  can be controlled using an error signal generated from a heterodyne beat between a cw optical frequency standard and one of the neighboring comb modes. This stabilization scheme comprises the basic gearwork for an optical atomic clock.

## 2.2. CONTROL OF COMB VIA AN OPTICAL CAVITY

A passive, high-finesse, and low-dispersion optical cavity is useful in many aspects to aid in high precision DFCS, as will be discussed in the following sections. A broad bandwidth optical frequency comb can be efficiently coupled into such a cavity, enabling its use as a frequency reference as well as enhancement of power and interaction length. Indeed, understanding the intricate interactions between a train of ultrashort pulses and passive optical cavities, along with the development of the capability to efficiently couple and coherently store ultrashort pulses of light inside a high-finesse optical cavity, has been an area of focused research (Jones and Ye, 2002). Several important studies have ensued. Intracavity storage and amplification of ultrashort pulses in the femtosecond regime require precise control of the reflected spectral phase of the resonator mirrors as well as the optical loss of the resonator. While the reflected phase and group delay of the mirrors only change the effective length of the resonator, the group delay dispersion (GDD) and higher-order derivatives of the group delay with respect to wavelength affect the pulse shape. The net cavity GDD over the bandwidth of the pulse needs to be minimized in order to maintain the shape of the resonant pulse and allow for the coherent addition of energy from subsequent pulses (Thorpe et al., 2005; Schliesser et al., 2006).

Direct stabilization of a frequency comb to a high-finesse optical cavity benefits from a low cavity dispersion that leads to a large spectral range over which comb and cavity modes can overlap precisely (Jones and Diels, 2001; Jones et al., 2004). A simplified schematic for cavity stabilization of femtosecond pulses is shown in Fig. 4. The pulse train is mode-matched to the passive high-finesse cavity after passing through an electro-optical phase modulator (EOM). Both  $f_r$  and  $f_o$  need proper adjustments to optimize frequency overlap between the comb components and the corresponding cavity modes. The light reflected from the cavity is spectrally dispersed with a grating and error signals from the cavity are obtained at different spectral regions resonant with the cavity ( $\omega_i$ ) using the standard Pound–Drever–Hall RF sideband technique (Drever et al., 1983).

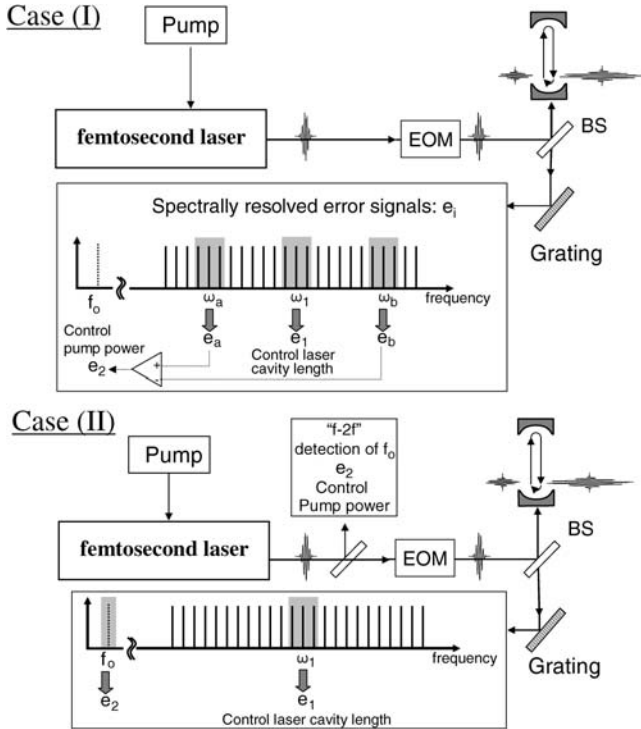


FIG. 4. Stabilization of a train of ultrashort pulses to a passive reference cavity. In scheme (I) “all-cavity locking”, both degrees of freedom of the fs frequency comb are detected with reference to the cavity and subsequently stabilized to the cavity. In scheme (II), an independent detection and stabilization of  $f_0$  is implemented using an octave-spanning comb bandwidth and an  $f$ -to- $2f$  interferometer.  $f_r$  is then stabilized via the cavity-generated error signal between a collection of comb components versus a corresponding set of cavity modes. In both panels, shaded regions indicate spectral positions at which the femtosecond comb is stabilized.  $e_i$ : error signal recovered at spectral region  $\omega_i$ ; BS: beam splitter; EOM: electro-optical modulator.

The error signals are then used to lock the two degrees of freedom of the frequency comb relative to the cavity. Two distinct stabilization schemes have been compared in detail, leading to the in-depth understandings of the optimum conditions for cavity stabilization of a frequency comb (Jones et al., 2004). In the first scheme, both error signals for comb stabilization are recovered from the cavity reference. The first error signal ( $e_1$ ) is obtained by comparing a collection of comb components (usually thousands of them) at the center of the spectrum ( $\omega_1$ ) against a corresponding set of cavity modes. This error signal can then be used to stabilize the length of the femtosecond laser cavity. To completely fix the comb, a second error signal ( $e_2$ ) is necessary, it is derived from a comparison of two

errors obtained at two spectral regions located symmetrically around the center, as shown in Fig. 4. The second error signal is used to control the laser cavity dispersion. In scheme (II), the second error signal is derived from a standard  $f$ -to- $2f$  self-referencing spectrometer, which corresponds to a direct detection and stabilization of  $f_o$ . The value of  $f_o$  is chosen to allow the maximum number of frequency comb modes to be matched to the cavity.

The stability of the frequency comb can be determined in both the optical and the radio frequency domains. It has been verified that the second scheme performed better than the first one due to the effective long “lever arm” (Jones et al., 2004). In principle, one could improve the performance of the first scheme by using a larger spectral separation between  $\omega_a$  and  $\omega_b$ . However, the ability to simultaneously optimize error signals in different spectral regions is necessarily limited by the parabolic variation of the cavity free-spectral-range (FSR) frequency, characteristic of the simple quarter-wave stack dielectric mirrors employed. By employing lower dispersion mirrors, the performance of the first scheme approaches that of the second. Using an independent, stable cw laser as a reference, measurement of the linewidth and stability of the cavity-stabilized optical frequency comb reveal superior performance comparable to that achieved by cavity-stabilized cw lasers.

The resulting frequency/phase stability between the frequency comb and the cavity modes demonstrates a fully coherent process of intracavity pulse buildup and storage. Similar to the state-of-art stabilization of cw lasers, a cavity-stabilized ultrafast laser demonstrates superior short-term stability of both  $f_r$  and  $f_o$ . The improved stability is beneficial for frequency-domain applications, where the relative phase or “chirp” between comb components is unimportant (e.g. optical frequency metrology), as well as time-domain applications where the pulse shape and/or duration is vital, such as in nonlinear optical interactions. These applications include optical frequency measurement, carrier-envelope phase stabilization, all-optical atomic clocks, optical frequency synthesizer, and coherent pulse synthesis.

To further improve the quality of femtosecond enhancement cavities, a femtosecond comb-based measurement protocol has been developed to precisely characterize mirror loss and dispersion (Thorpe et al., 2005; Schliesser et al., 2006). This technical capability has facilitated production of large bandwidth, low-loss and low-dispersion mirrors. In addition, nonlinear responses of intracavity optical elements have been studied, demonstrating their limitation on power scalability (Moll et al., 2005). This study has led to the design of novel cavity geometries to overcome this limitation (Moll et al., 2006). In short, nearly three-orders of power enhancement inside a femtosecond buildup cavity within a spectral bandwidth of 30 nm has been achieved, resulting in an intracavity pulse train that (1) is completely phase coherent to the original comb from the oscillator, (2) has the original laser’s repetition rate (100 MHz), (3) has a pulse peak

energy exceeding 5  $\mu\text{J}$  (average power  $> 500$  W), intracavity peak intensity approaching  $10^{14}$  W/cm<sup>2</sup>, and (4) is under 60 fs pulse duration. We also note that this enhancement cavity approach is compatible with a number of femtosecond laser systems, including mode-locked Ti:sapphire and fiber lasers.

The use of power-enhanced intracavity pulses for high harmonic generation will be discussed in Section 6.2. This is partly motivated by the fact that coherent optical spectroscopy has now led to the recovery of a record-high quality factor ( $Q > 2.4 \times 10^{14}$ ) for a doubly “forbidden” natural resonance observed in a large ensemble of ultracold Sr atoms trapped in an optical lattice (Boyd et al., 2006). This unprecedented spectral resolving power impacts fields ranging from precision frequency metrology to quantum optics and quantum information science. Ultrastable lasers, together with optical frequency combs, can now maintain optical phase coherence beyond 1 s and transfer this stability across hundreds of terahertz (Bartels et al., 2004a; Ludlow et al., 2006). As it becomes increasingly challenging to maintain phase coherence beyond multiple seconds, it is natural to look beyond the visible domain and consider speeding up the “wheel of precision measurement” to higher carrier frequencies. Two related experimental directions are currently being pursued to address this vision. One is the generation of phase coherent, high repetition-rate frequency combs in the VUV (50–200 nm) spectral domain (Jones et al., 2005; Gohle et al., 2005). In parallel, direct frequency comb spectroscopy (Marian et al., 2004) is being explored to ready ourselves for quantum optics and precision spectroscopy once phase coherent sources (necessarily in the form of a train of pulses) become available in VUV. In addition to the power enhancement aspect, a femtosecond cavity effectively increases the interaction length between matter and light, allowing direct frequency comb spectroscopy to measure weak linear or nonlinear atomic and molecular absorption with dramatically increased sensitivity and across a vast spectral bandwidth (Thorpe et al., 2006, 2007).

The coherently enhanced pulse train stored in the cavity can also be switched out using a cavity-dumping element (Bragg cell), resulting in phase-coherent, amplified pulses at a reduced repetition frequency (Potma et al., 2003; Vidne et al., 2003; Jones and Ye, 2004). The net cavity group delay dispersion over the bandwidth of the pulse is minimized to maintain the shape of the resonant pulse. This coherent pulse-stacking technique has been applied to both picosecond (Potma et al., 2003) and femtosecond pulses (Jones and Ye, 2004), demonstrating amplifications  $> 500$ . An important application of these advanced pulse-control technologies is in the field of nonlinear optical spectroscopy and nanoscale imaging. Using two tightly synchronized picosecond lasers, one can achieve a significant improvement in experimental sensitivity and spatial resolutions for vibrational imaging based on coherent anti-Stokes Raman spectroscopy (CARS) for acquisition of chemically selective maps of biological samples (Potma et al., 2002,

2004). The technologies of pulse synchronization and coherent pulse stacking fit well with this task of combining spectroscopy and microscopy.

### 3. Direct Frequency Comb Spectroscopy

Femtosecond lasers have been used to reveal ultrafast dynamics and provide wide bandwidth spectroscopic information in atomic, molecular, and condensed matter systems (Zewail, 2000; Jonas, 2003). The advent of precision femtosecond optical combs brings a new set of tools for precision atomic and molecular spectroscopy. For example, ultrafast lasers are now being used not only for time-resolved spectroscopy on fast dynamics, but also for precision spectroscopy of electronic transitions. Indeed, coherent control of dynamics and precision measurement are merging into a joint venture (Stowe et al., 2006). The ability to preserve optical phase coherence and superior spectral resolution over a wide spectral bandwidth permits detailed and quantitative studies of atomic and molecular structure and dynamics. The spectral analysis can be performed over a broad wavelength range, allowing precise investigations of minute changes in atomic and molecular structure over a large dynamic range (Chen and Ye, 2003). For example, absolute frequency measurement of vibration-overtone transitions and other related resonances (such as hyperfine splitting) can reveal precise information about the molecular potential-energy surface and relevant perturbation effects (Chen et al., 2004, 2005).

With precise control of both time- and frequency-domain properties of a pulse train, these two features can be combined into a single spectroscopic study, as demonstrated in the following sections. The broad frequency comb bandwidth available for modern comb spectroscopy measurements distinguishes them from the earlier picosecond-pulse based experiments, leading to truly united time-frequency spectroscopy for broad-bandwidth spectroscopy (Marian et al., 2004). Precision spectroscopy of global atomic structure is achieved with a direct use of a single, phase-stabilized femtosecond optical comb. The pulsed nature of excitation allows real-time monitoring and control capabilities for both optical and quantum coherent interactions and state transfer. It is a synthesis of the fields of precision spectroscopy and coherent control: at short time scales the coherent accumulation and population transfer is monitored, at long times all the information pertinent to the atomic level structure is measured at a resolution limited only by the natural atomic linewidth, with a spectral coverage spanning hundreds of terahertz. This powerful combination of frequency-domain precision and time-domain dynamics represents a new paradigm for spectroscopy.

The precision and control of both the frequency and time domain achievable with femtosecond frequency combs introduce many new features to spectroscopy. In particular the spectroscopic resolution and precision are not compromised by

the use of the inherently spectrally broad ultrafast pulses. This is due to the long coherence time of the phase-stabilized femtosecond pulse train. Also, no prior knowledge of atomic transition frequencies are essential for this technique to work. The results presented in this chapter demonstrate the revolutionary advantage of direct frequency comb spectroscopy (DFCS), i.e., the comb frequencies may be absolutely referenced, for example to a cesium atomic clock, enabling absolutely referenced precision spectroscopy over a bandwidth of several tens of nanometers (Marian et al., 2004, 2005; Mbele et al., in preparation). Furthermore, spectral phase manipulation can now be combined with the time-domain optical phase coherence to enable quantum coherent control at resolutions limited only by the natural linewidth (Stowe et al., 2006). Indeed, the field of coherent control of atomic and molecular systems has seen advances incorporating high power femtosecond laser sources and pulse shaping technology. As will be discussed further, this has allowed for demonstrations of robust coherent population transfer via adiabatic passage techniques, coherent control of two-photon absorption, resolution enhancement of coherent anti-Stokes Raman scattering, and progress toward cold atom photoassociation.

### 3.1. THEORETICAL TREATMENTS

The theoretical work for modeling the interaction of pulsed optical fields with atoms has been explored in several directions. Most treatments focus primarily on the interaction of broad-bandwidth pulses with two or three level atoms and neglect propagation effects and the motional degrees of freedom of the atom. We briefly present an overview of some work done concerning effects not directly addressed in this review. Perhaps the most fundamental question is how does a few cycle femtosecond pulse interact with a two-level atom. The works of Genkin (1998), Casperson (1998) address this question and the limits of common approximations such as the rotating wave approximation. Concerning pulse propagation, work has been done illustrating pulse shaping effects and the pulse area theorem applied to ultrashort pulses (Delagnes et al., 2003; Ziolkowski et al., 1995). Analytic expressions for the excitation of a two-level atom by a train of pulses have been derived in Vitanov and Knight (1995), Greenland (1983).

For much of the experimental work reviewed in this chapter the relevant physics is the single and multi-photon absorption in multi-level atoms or molecules from an optical pulse train of moderate intensity. The root concept behind direct frequency spectroscopy can be found in Ramsey spectroscopy, see Fig. 1, in which only two narrow band pulses excite the atom. Basically, the first broadband pulse excites a small fraction of population to all allowed transitions within the pulse bandwidth. The second and subsequent pulses interact with the coherences generated by the first pulse and, depending on the relative phase of the pulse with

the coherence, population is either excited or de-excited. We refer to the coherent interaction of a series of pulses with an atomic or molecular transition as coherent accumulation. This is the key physical concept behind the signal size and resolution enabled by DFCS. To excite only one of many states in the bandwidth of the pulse,  $f_o$  and  $f_r$  may be chosen to always be in phase with only one coherence. In the frequency-domain picture this is simply to say one comb mode is resonant and all others are detuned. To properly treat multi-photon absorption the sum of comb modes must be considered, for example in a two-photon transition there may be hundreds of thousands of resonant mode pairs. Due to the fact that more than one pair of modes may excite a two-photon transition the spectral phase of each mode, and intermediate state detunings, must be considered to account for quantum interference effects.

Two models are used for the majority of the theoretical predictions for the experiments presented in Sections 3.2 and 3.3. The first is a perturbative model suitable for two-photon absorption of transform limited pulses in multi-level atoms, for example the many hyperfine levels of the 5S, 5P, and 5D states of rubidium 87. This technique, presented by Felinto et al. (2004), uses the impulsive excitation approximation such that the spectral content and phase of the pulse are not included. It provides a computationally fast method to predict the complicated optical pumping effects present between the many comb modes and electronic states. Other experiments require either a non-perturbative treatment or the capability of modeling spectral phase effects for multi-photon absorption. In this case one can directly numerically solve the Liouville equation for the density matrix of the system for a three-level model under arbitrary shaped pulse excitation. The advantage of this approach is that it correctly predicts pulse shaping effects on multi-photon transitions and the non-perturbative effect of power broadening of atomic transitions relevant to correctly modeling parts of Sections 3.3 and 5.

In many experiments it is possible to treat only those comb modes that are resonant with a transition. The simplest case is when the comb is tuned to be resonant with only one single-photon transition and the nearest mode for all other transitions is detuned several linewidths. Similarly, for a resonantly enhanced two-photon transition it may be reasonable to analytically model the interaction using only the two resonant modes. The two-photon transition amplitude,  $C_{gf}$ , useful for calculating most results in Section 3.3 is,

$$\begin{aligned}
 C_{gf} \propto & \frac{E_n E_m}{i(\omega_{gf} - (m+n)2\pi f_r - 4\pi f_o) + \pi \gamma_f} \\
 & \times \left( \frac{1}{i(\omega_{gi} - 2\pi(nf_r + f_o)) + \pi \gamma_i} \right. \\
 & \left. + \frac{1}{i(\omega_{gi} - 2\pi(mf_r + f_o)) + \pi \gamma_i} \right)
 \end{aligned} \tag{1}$$

where  $E_{n,m}$  are the electric fields of the  $n$ th and  $m$ th modes of the comb,  $\gamma_i(f)$  is the intermediate (final) state scattering rate,  $\omega_{gi(gf)}$  is ground to intermediate (final) state transition frequency. In general, the total transition amplitude is the sum over all modes of the comb and intermediate states. The full equation with comparison to time-domain techniques may be found in [Yoon et al. \(2000\)](#).

In molecular systems, where the number of individual states covered by the bandwidth of the pulses may be too large to handle by direct solution in state space, one can use techniques developed for the modeling of wave-packet dynamics, such as the split-operator method. In these techniques, one directly solves the time-dependent Schrödinger equation with a set of electronic potentials coupled by the time-dependent fields of the pulses, see [Garraway and Suominen \(1995\)](#) for a comprehensive review. The theoretical results shown in Section 5.2 were obtained with such a model. Like in the case of atomic excitation, the coherent accumulation was modeled by simulating a single femtosecond pulse interaction followed by free evolution of the molecular coherences between pulses, this procedure is then repeated for every pulse.

### 3.2. SINGLE-PHOTON DFCS

Of the many applications directly using the output of a femtosecond laser frequency comb (FLFC) for spectroscopy, single-photon spectroscopy is the easiest to realize experimentally. A single frequency component of the broad comb spectrum is used to selectively excite an atomic or molecular transition. The spectra are recorded by measuring the excited-state fluorescence while changing the laser's repetition rate  $f_r$  or carrier-envelope offset frequency  $f_o$ . The time-domain properties of the laser determine only the frequency and width of the selected component, but the requirements for pulse overlapping or preserving the phase relation across multiple comb components are relaxed. The femtosecond laser frequency comb can be viewed simply as a multimode laser with narrow-linewidth modes at known optical frequencies. As a result, all methods of cw laser spectroscopy can be applied with the advantage of absolute frequency calibration determined by the knowledge of  $f_r$  and  $f_o$ . Additionally, the combs have spectral components where no tunable cw laser sources exist, and they cover a broad spectral interval allowing spectroscopy of different atomic or molecular systems to be done with the same laser system. In particular the high peak intensity attainable with femtosecond pulses allows for efficient nonlinear conversion to spectral regions with difficult or no accessibility by traditional cw laser techniques, see Section 3.4 for a specific example.

Several disadvantages of using FLFC for single-photon spectroscopy have to be mentioned. The total laser intensity is distributed among  $\sim 10^5$  comb modes, resulting in a per mode intensity typically below 1  $\mu$ W. Consequently spectroscopy

must be performed with very low laser power levels. This limits the sub-Doppler spectroscopy experiments to atomic beams or laser cooled systems, where the Doppler width has already been reduced geometrically or using laser cooling (Gerginov et al., 2005; Marian et al., 2004). Saturated absorption is possible, but in order to reach significant saturation, tight laser beam focusing is required which leads to time of flight broadening and other systematic effects. A possible solution to the low intensity problem is amplification of the comb's output, as shown in Section 3.2.3.

When the repetition rate is swept in order to measure the atomic transition spectrum, the same difficulties as when using multimode lasers are encountered. Due to interleaving, all spectral features will be present in a frequency window determined by the separation of the comb components at the optical frequency of interest. The identification of the spectral lines becomes problematic. The presence of many other comb components, even if filtered by an interference filter or using techniques described in the sections below, leads to systematic effects such as AC Stark shifts. It is difficult to directly measure the intensity of any single comb mode, although it may be inferred from the laser's spectral shape, power, and mode separation. The method of measuring the excited population in the following experiments is either directly via fluorescence or population transfer with a cw probe laser. This is preferable because in transmission, all components present in the comb spectrum contribute to the background.

Determining the absolute frequency of a transition measured by DFCS requires the determination of the resonant comb mode index,  $n$ . There are generally two ways to determine the index. In some applications the frequency may be already known to within half the comb mode spacing. If this is the case then it is trivial to unambiguously determine  $n$  and calculate the absolute transition frequency using  $\nu_n = nf_r + f_o$ . The second more general technique is to measure the linecenter with two or more different  $f_r$ . In principle, that is in the absence of uncertainty corresponding to the  $f_o$  and  $f_r$  of the measured linecenter, the idea is straightforward. Measure the linecenter with  $\nu_n = nf_r + f_o$  and  $\nu_n = n(f_r + \Delta f_r) + (f_o + \Delta f_o)$ , where  $\Delta f_r$  is small enough such that the resonant mode remains the same. From these measurements it is clear  $n = -\Delta f_o / \Delta f_r$ . In practice there is measurement uncertainty and  $\Delta f_r$  must be made larger, in general the resonant comb mode will change but  $\Delta n$  may be determined. Cases may also arise in which two different atomic transitions are spaced by approximately  $f_r$ , these lines would overlap and it may be necessary to choose an appropriate  $f_r$  range, or filter the pulse spectrum, to reduce the congestion of resonant transitions.

### 3.2.1. Single-Photon Spectroscopy of Rubidium

The first DFCS experiment we discuss measured the 5S to 5P single-photon transitions in laser cooled  $^{87}\text{Rb}$  atoms (Marian et al., 2005). This simple application

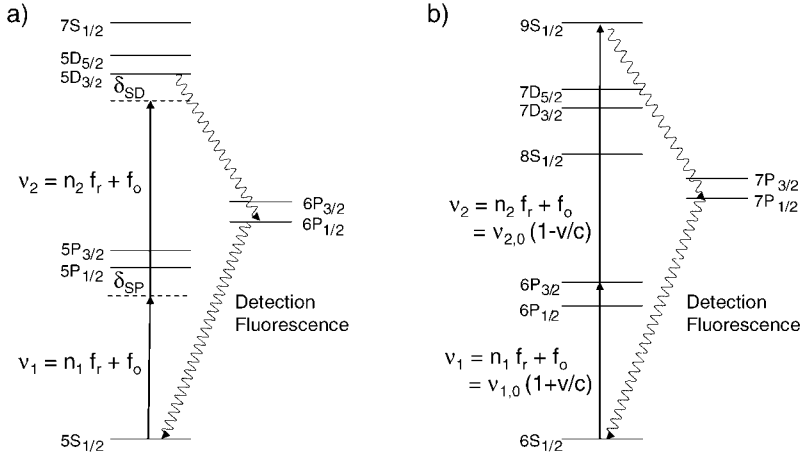


FIG. 5. Relevant energy levels studied in experiments in (a) Rb and (b) Cs. The two-photon transitions reached by two modes of the comb are discussed in Section 3.3. Although not shown the comb resolution allows the excitation of specific hyperfine levels.

is a clear demonstration of how DFCS can be used to determine the absolute frequency of any allowed transition within the laser bandwidth, see Fig. 5(a). A mode-locked Ti:sapphire laser operated at 100 MHz repetition rate, outputting 20 fs pulses, with a center wavelength of 780 nm was used to excite a sample of <sup>87</sup>Rb atoms in a magneto-optical trap (MOT). A crystal oscillator with low short-term instability was used to lock  $f_r$  resulting in a comb mode linewidth of 330 kHz at 1 ms integration time. To absolutely reference the frequencies of the comb modes  $f_r$  was measured on a cesium referenced counter and steered appropriately. To shutter the fs probe pulses a Pockels cell with an 8 ns rise time was used. In brief, the experimental cycle generally used was as follows: the MOT was loaded for 7.8 ms, the magnetic field was turned off and the atoms were held in optical molasses for 2 ms, then all MOT related optical fields were extinguished before probing the atoms for 200  $\mu$ s. Weakly focusing the fs pulses into the MOT to a diameter of about 130  $\mu$ m results in an on axis average intensity of 0.8 mW/cm<sup>2</sup>. Due to the fact that the 5P fluorescence is at a wavelength present in the pulse spectrum the photomultiplier tube used to measure the fluorescence signal is turned off during the excitation time to avoid background counts. Similarly the fs laser was shuttered during the PMT operation time. Within the 200  $\mu$ s probing window the atoms were repeatedly excited and then PMT was used to count the 5P fluorescence signal immediately after excitation. The  $f_r$  and  $f_o$  of the comb were chosen such that only the 5S<sub>1/2</sub> $F = 2$  to 5P<sub>3/2</sub> $F = 3$  transition is near resonance, all other transitions are several linewidths detuned. Figure 6(b) shows the measured lineshape recovered by scanning  $f_o$  and translat-

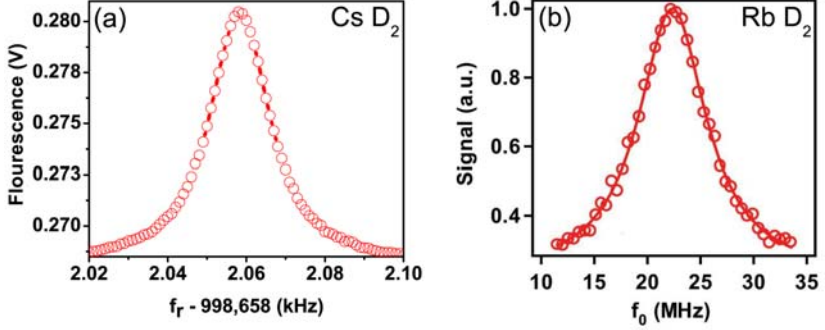


FIG. 6. (a)  $^{133}\text{Cs}$   $D_2$   $F = 4 \rightarrow F = 5$  line scan versus  $f_r$  with  $f_o = 120$  MHz and 1.5 nW/mode. (b)  $^{87}\text{Rb}$   $D_2$   $F = 2 \rightarrow F = 3$  line scan versus  $f_o$  with  $f_r$  fixed.

ing the resonant comb mode over the atomic transition. To minimize any Doppler shift of the linecenter versus time, from repeated scattering via  $5P_{3/2}F = 3$ , the pulses were counter-propagated through the atoms balancing the radiation pressure. However, there is still residual radiation pressure that causes the linecenter to shift versus probing time. Taking this into account the linecenter versus time is measured and extrapolated to zero probing time to recover a center frequency of  $\nu = 384, 228, 115, 271(87)$  kHz.

The broad bandwidth of a Ti:sapphire frequency comb has also recently been used to study velocity selective excitation of a room temperature cell of Rb atoms, see the work of [Aumiler et al. \(2005\)](#), [Ban et al. \(2006\)](#). In these experiments the Doppler broadening at room temperature is significantly larger than the intermode spacing of the frequency comb used for excitation. This leads to a velocity selective excitation and optical pumping of both the ground and excited  $5P$  state hyperfine levels. By measuring the absorption profile versus frequency with a separate cw laser several transparency windows are observed corresponding to different velocity classes of the thermal Rb ensemble. Similar experiments have been performed that used significantly narrower bandwidth mode-locked lasers to demonstrate electromagnetic induced transparency (EIT) with a comb ([Sautenkov et al., 2005](#); [Arissian and Diels, 2006](#)). The idea is very similar to the work discussed in Section 1. By tuning the inter-pulse period or  $f_r$  to a harmonic of the ground state hyperfine splitting the atoms can be driven into a dark state. Future experiments in this direction may lead to the ability to directly lock  $f_r$  of the comb to the narrow transparency window achievable with EIT.

### 3.2.2. Single-Photon Spectroscopy of Cesium

Another experiment demonstrating single-photon spectroscopy in  $^{133}\text{Cs}$  is done using a thermal atomic beam. It uses a self-referenced Ti:sapphire femtosec-

ond laser frequency comb with a 1 GHz repetition rate (Ramond et al., 2002; Bartels et al., 2004a; Gerginov et al., 2005). Its repetition rate,  $f_r$ , and the carrier-envelope offset frequency,  $f_o$ , of the femtosecond laser are phase-locked to frequency synthesizers referenced to a stable hydrogen maser, which is calibrated by a cesium atomic fountain clock (Heavner et al., 2005; Ramond et al., 2002; Morgner et al., 2001). The fractional frequency instability of the comb teeth is determined by that of the hydrogen maser, given by  $\sim 2 \times 10^{-13} \tau^{-1/2}$ , where  $\tau$  is the integration time measured in seconds. A single-mode fiber is used to deliver part of the comb's output to the highly-collimated atomic beam (Gerginov et al., 2004). The optical power is stabilized using the zero diffraction order of an acousto-optical modulator (AOM), placed before the optical fiber. It should be noted that for single-photon absorption spectroscopy the spectral phase of the femtosecond pulses does not effect the signal strength, therefore pulse stretching in, for example, the fiber or AOM is of no concern. However, in multi-photon absorption the spectral phase may be of importance and will be addressed in Section 5.

To excite the  $6s^2S_{1/2} \rightarrow 6p^2P_{1/2}$  ( $D_1$ ) and  $6s^2S_{1/2} \rightarrow 6p^2P_{3/2}$  ( $D_2$ ) lines in Cs, the comb spectrum was filtered using interference filters centered at 900 and 850 nm, respectively. The Cs atomic beam is collimated to a rectangular profile. The output of the single-mode fiber is collimated and intersects the thermal atomic beam at a right angle after the nozzle and above a large-area photodetector.

Around 895 nm, the FLFC excites four different components of the transition  $6s^2S_{1/2} (F_g = 3, 4) \rightarrow 6p^2P_{1/2} (F_e = 3, 4)$ . Due to the presence of a comb tooth every 1 GHz, the fluorescence signals also repeat every 1 GHz change in optical frequency (interleaving), corresponding to a change in  $f_r$  of  $\sim 3$  kHz.

The FLFC spectrum, narrowed in the vicinity of 850 nm, excites six components of the transition  $6s^2S_{1/2} (F_g = 3, 4) \rightarrow 6p^2P_{3/2} (F_e = 2, 3, 4, 5)$ . The fluorescence versus femtosecond laser repetition rate for one of the Cs  $D_2$  lines is shown in Fig. 6(a).

In this measurement, previous knowledge of the optical frequencies were used to identify each spectral component. Due to the large repetition rate of the femtosecond laser (1 GHz), such identification is possible knowing the optical frequencies with a precision of several tens of megahertz, significantly better than  $f_r/2$ . As previously mentioned using different repetition rates of the femtosecond laser to measure the same spectra, identification without previous knowledge of optical frequencies is possible (Halzwarth et al., 2001; Ma et al., 2003; Marian et al., 2005).

Due to reduced signal-to-noise ratio in the FLFC experiment, the AC Stark shift of the optical frequency was not measured. The first-order Doppler shift was canceled with the technique described in detail in Gerginov et al. (2004, 2006). Due to the reduced signal-to-noise ratio, this cancellation is limited by the statistical uncertainty in the optical frequency determination, and is probably the reason

for the small offset of the FLFC data compared with the one obtained with the CW laser. From the data presented in [Gerginov et al. \(2005\)](#), it is clear that the statistical and fit uncertainties approach the ones obtained using a cw laser.

### 3.2.3. Excitation of Forbidden Transitions

An extension of the ideas and techniques of single-photon spectroscopy described above to the study of forbidden transitions requires additional considerations. In particular, the difficulties encountered due to the small power per optical mode are heightened. Two possible solutions to this problem are the use of cold atoms, which allow for long interrogation times, and the amplification of the comb. In addition to the power considerations, the study of forbidden transitions also requires the optical comb modes to be narrower than what is needed for the study of dipole-allowed transitions. Thus, the stabilization of the comb's repetition rate directly to an RF source is insufficient and greater stability can be achieved by stabilizing a single optical mode to a highly stable laser, in addition to the usual stabilization of the carrier-envelope offset frequency. These extensions were demonstrated in the context of studying the narrow  $4s^2\ ^1S_0 \rightarrow 4s4p\ ^3P_1$  transition in calcium (Ca) ([Fortier et al., 2006b](#)).

The experimental setup for the experiment of Fortier and co-workers is shown in [Fig. 7](#). The  $4s^2\ ^1S_0 \rightarrow 4s4p\ ^3P_1$  transition in Ca is forbidden in the spin-orbit

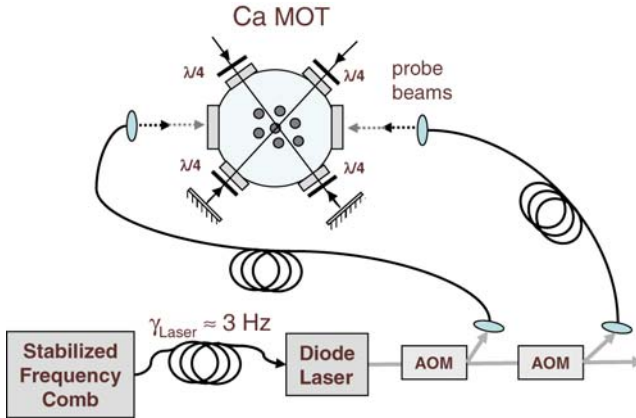


FIG. 7. Experimental depiction for high-precision optical spectroscopy of cold Ca atoms using a femtosecond laser frequency comb. Acousto-optical modulators (AOM) switched light between two optical fibers that deliver counter-propagating pulses to the Ca magneto-optical trap (MOT). An  $f$ -to- $2f$  self-referencing technique allows phase stabilization of the laser offset frequency,  $f_o$ . Phase stabilization of the laser repetition rate,  $f_r$ , is obtained by phase locking the comb to a fiber laser at 1068 nm that is stabilized to a high-finesse optical cavity. Measurement of the laser repetition with respect to a hydrogen-maser provided absolute frequency calibration in the measurements.

approximation and has a natural linewidth of 374 Hz (Degenhardt et al., 2005), and this transition has been studied extensively as an optical frequency standard (Degenhardt et al., 2005; Oates et al., 2000). In this experiment, the frequency comb was derived from an octave-spanning mode-locked Ti:sapphire laser with a  $\approx 1$  GHz repetition rate (Fortier et al., 2006a). Due to the transmission of the output coupler, the output power of the laser peaked around the 657 nm wavelength needed to excite the  $4s^2\ ^1S_0 \rightarrow 4s4p\ ^3P_1$  transition. The power per mode at this wavelength was  $\approx 1\ \mu\text{W}$ . With this type of power and the small dipole matrix element of the transition, one has Rabi frequencies of  $\sim 10$  kHz. In order to achieve sizable population transfer, it is necessary to have interrogation times of  $\sim 10\ \mu\text{s}$ . These types of interrogation times can be achieved with moderately cooled atoms with temperatures of a few millikelvin.

Because the frequency comb was in a different laboratory from the Ca atoms it was necessary to fiber couple the comb light. In addition, the light was passed through an AOM to allow for switching of the light. In order to overcome the losses introduced by these processes, the frequency comb light was amplified by using the comb light to injection lock a diode laser (Cruz et al., 2006). Two regimes of amplification were observed depending on the current applied to the slave diode. With the current of the slave diode near the lasing threshold, the  $\approx 0.5$  nm of injected light was amplified more or less uniformly, providing an amplification factor of  $\sim 10$ . This amplification compensated for the losses described above and allowed for saturation spectroscopy of the transition and observation of the photon-recoil splitting (Hall et al., 1976; Oates et al., 2005), see Fig. 8(a). With the current of the slave diode significantly above the lasing threshold, the amplification was dominated by specific optical modes. By fine adjustment of the diode current and temperature, it was possible to preferentially amplify the optical mode resonant with the transition. In this regime, an amplification of  $\sim 2000$  was observed. This amplification was sufficient to observe the Ramsey–Bordé fringes (Bordé et al., 1984) and achieve spectral resolutions of 1 kHz, see Fig. 8(b).

In addition to the restrictions imposed by the low optical powers available, the study of forbidden transitions requires that the individual optical modes be narrower than is necessary for the study of allowed transitions. If the repetition rate is stabilized directly to an RF source, any noise present in the RF source is multiplied by the optical mode number. This places stringent requirements on the short-term stability of the RF source if the comb is to be used to study narrow transitions. This problem can be circumvented by instead stabilizing a single comb mode, with mode number  $n$ , to a stable cw laser of frequency  $\nu_{cw}$ . The frequency of a given comb mode,  $m$ , is then given by

$$\nu_m = \frac{m}{n}(\nu_{cw} + f_b) + f_o \left(1 - \frac{m}{n}\right), \quad (2)$$

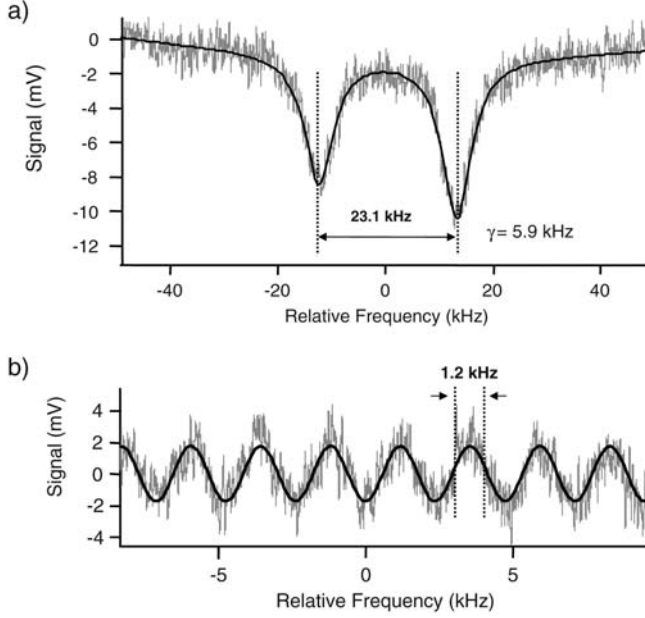


FIG. 8. (a) Saturation absorption dip observed on the Doppler profile of the Ca clock transition using two counter-propagating pulses. The double peak is the photon-recoil doublet. (b) Time-resolved optical Bordé-Ramsey fringes.

where  $f_b$  is the heterodyne beat signal between the comb mode  $n$  and the cw laser. The frequency  $\nu_m$  can be scanned by changing the frequency of the heterodyne beat note  $f_b$  while the frequency comb is stabilized to light from a cw fiber laser at 1068 nm. The cw fiber laser was stabilized by doubling a portion of the light and referencing it to an ultrastable optical cavity (Young et al., 1999). The residual linewidth of the light at 1068 nm was  $\sim 1$  Hz. This stability was transferred to the entire bandwidth of the comb, providing a sufficiently narrow linewidth for the spectroscopy of the  $4s^2 \ ^1S_0 \rightarrow 4s4p \ ^3P_1$  transition.

### 3.3. MULTI-PHOTON DFCS

Direct frequency comb spectroscopy is not only useful for single-photon transitions but also multi-photon transitions. Two general cases exist in the context of two-photon transitions, those with an intermediate resonance and those in which the pulse spectrum is far detuned from an intermediate resonance. In the case where one mode is resonant with the intermediate state, the system can often be understood by considering only two modes. However, when there is no interme-

diate resonance in the spectrum it should be noted that if one pair of comb modes is two-photon resonant, then all modes will form a resonant pair due to the equal spacing of modes.

### 3.3.1. Multi-Photon DFCS of Rubidium

The following experiment demonstrates the versatility of DFCS for measuring two-photon transitions. The absolute transition frequencies of several hyperfine levels in the 5D and 7S manifolds were measured, via resonant enhanced transitions through an intermediate 5P hyperfine level (Marian et al., 2004, 2005). Primary focus was placed on the  $5S_{1/2}F = 2 \rightarrow 5P_{3/2}F = 3 \rightarrow 5D_{5/2}F = 4$  transition because it is the strongest transition in the comb bandwidth. This is due to the fact it has the highest dipole moments, and the  $5P_{3/2}F = 3$  level may only decay to  $5S_{1/2}F = 2$ , avoiding excessive optical pumping to off resonant levels. The setup is essentially the same as the one used for measuring single-photon transitions in laser cooled  $^{87}\text{Rb}$  described in Section 3.2.1. One difference is that the population of the 5D or 7S states was determined by monitoring the fluorescence at 420 nm resulting from the cascade decay of the 6P state to the 5S state. There are a total of 14 transitions between the 5S and 5D states alone, this large number of possible transitions makes for an excellent DFCS demonstration using different comb modes from one laser for spectroscopy.

Figure 9 shows the measured signal, proportional to the 5D population, versus a scan of  $f_r$  by only 26 Hz while keeping  $f_o$  fixed. Within this one scan it is possible to identify 28 lines. The optical frequency for the two-photon transition is of the order 770 THz, this corresponds to a  $f_r$  harmonic of  $7.7 \times 10^6$ , dividing  $f_r \cong 100$  MHz by this value gives a value of  $\Delta f_r = 13$  Hz before the next comb mode becomes resonant with any given transition. The single-photon transition being at approximately  $\frac{1}{2} \times 770$  THz repeats after every 26 Hz change of  $f_r$ . Identified in Fig. 9 are the single-photon resonant and detuned lines, thus 28 lines for 14 possible transitions, although in this range of  $f_r$  some lines overlap. Several transition frequencies for both one- and two-photon absorption are provided in Table I.

As an explicit experimental demonstration of the resolution and signal enhancement of multi-pulse coherent accumulation, the  $5S_{1/2}F = 2 \rightarrow 5P_{3/2}F = 3 \rightarrow 5D_{5/2}F = 4$  transition is measured versus a controllable number of pulses (Stowe et al., 2006). A Pockels with a 8 ns rise time is used as a pulse picker and triggered in phase with  $f_r$  such that any number of pulses can be used to excite the atoms. Figure 10 shows the resulting  $5D_{5/2}F = 4$  population and lineshape versus pulse number, rescaled to match the theoretical predictions. Perhaps the clearest example of coherent accumulation, shown in the inset of Fig. 10, is the quadratic scaling of population at short times, or pulse number. This is because the total accumulated pulse area prior to atomic decoherence is the sum of the

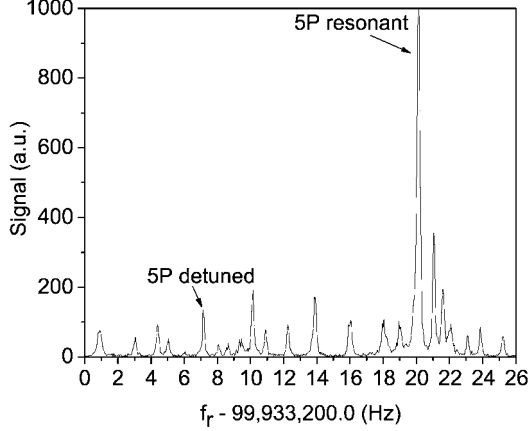


FIG. 9. Full spectrum of all allowed two-photon transitions from  $5S \rightarrow 5D$  of  $^{87}\text{Rb}$ . This spectrum was measured in only a 26 Hz scan of  $f_r$ . Different modes of the comb become resonant with transitions at various values of  $f_r$  allowing for large spectral coverage. Two peaks are identified in the figure both corresponding to the  $5S_{1/2}F = 2 \rightarrow 5P_{3/2}F = 3 \rightarrow 5D_{5/2}F = 4$  transition. The larger of the two peaks is exactly resonant with both the single- and two-photon transitions. The weaker line, although two-photon resonant, is off resonant with any intermediate states.

Table I

Rubidium two-photon transition frequencies measured by DFCS

Measured transition (from $5S_{1/2}F = 2$ )	Measured frequency (kHz)
$5D_{5/2}F = 2$	770,569,184,527.9 (49.3)
$5D_{5/2}F = 3$	770,569,161,560.5 (11.1)
$5D_{5/2}F = 4$	770,569,132,748.8 (16.8)
$5D_{3/2}F = 3$	770,480,275,633.7 (12.7)
$5D_{3/2}F = 2$	770,480,231,393.9 (38.1)
$5P_{3/2}F = 3$	384,228,115,309.0 (63.0)
$5P_{1/2}F = 2$	377,105,206,938.7 (179.0)

individual pulse areas. In analogy with driving a two-level system with a resonant cw laser the population initially scales as the square of time, or equivalently as the square of accumulated area. At longer times, or larger number of pulses, the decoherence due to the natural lifetime of the  $5D$  state begins to limit the coherent accumulation until eventually steady state is reached. In this experiment the resonant comb modes are strong enough to cause substantial power broadening of the measured linewidth. As can be seen in Fig. 10 the linewidth clearly becomes narrower as more pulses are coherently accumulated, eventually reaching

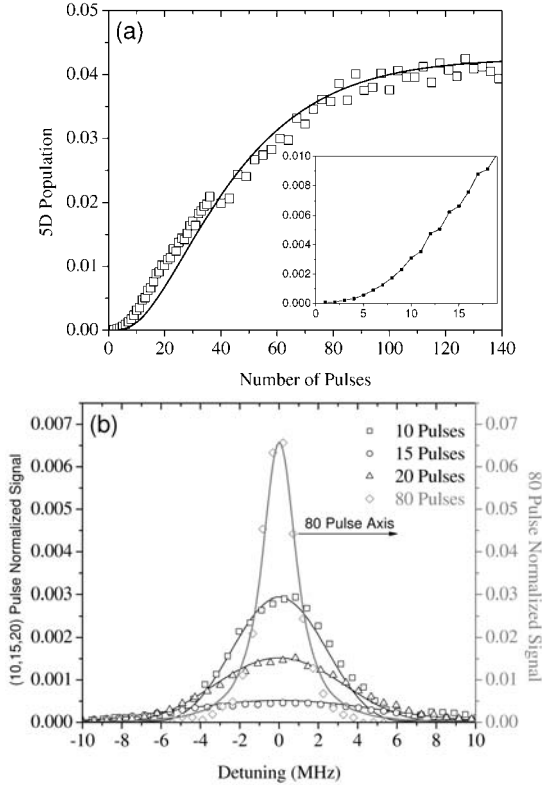


FIG. 10. Shown in (a) is the excited state population versus pulse number. Notice two features in particular, for short times the scaling is quadratic versus pulse number (see inset), and the population reaches steady state at approximately 80 pulses. Scanning  $f_o$  recovers the lineshape versus pulse number shown in (b). The power broadened asymptotic linewidth of 2.2 MHz is reached at approximately 80 pulses.

the asymptotic power broadened linewidth of 2.2 MHz at 80 pulses. In principle the resolution obtainable by DFCS is only limited by decoherence mechanisms, typically due to the atomic transition because modern fs comb linewidths can be reduced to the 1 Hz level.

To determine the linecenter with high accuracy it is necessary to conduct a higher resolution scan of the line of interest. Several sources of systematic error must be carefully addressed to determine the unperturbed linecenter of interest. For all measurements the fs pulses are counter-propagated through the same set of atoms within the MOT to balance the radiation pressure. Provided the intensities of the two counter-propagating beams are well matched the net momentum transfer along the probing direction via photon scattering, primarily from the 5P

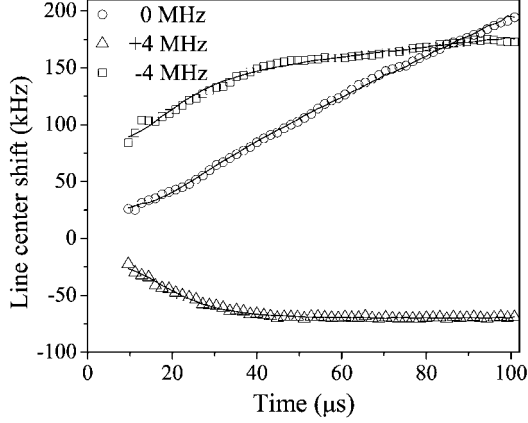


FIG. 11. The measured linecenter shift of the  $5D_{5/2}F = 4$  level versus time relative to an arbitrary reference value. For times below approximately  $40 \mu\text{s}$  the fs comb power is increasing as the LCD shutter used in this experiment turns on, after  $40 \mu\text{s}$  the power is constant. Three cases are presented for different intermediate state detunings, all are nominally on resonance with  $5D_{5/2}F = 4$ . Two effects may be seen in this data, first the Stark shift is approximately equal and opposite about the 0 MHz detuning result for the  $\pm 4$  MHz detuning cases. Secondly, notice when the fs comb power is constant the Stark shift is constant (red and blue detunings). However, the on resonance case undergoes significant accumulative Doppler shift due to radiation pressure from the residual intensity and alignment mismatch between the counter-propagating probe beams.

states, is significantly reduced. Repeated scattering also heats the atomic ensemble, broadening the linewidth. Similarly a residual net intensity imbalance of the probe beams can accelerate the atoms resulting in a Doppler shift of the measured linecenters. The linecenter results reported in this review are based on measuring and fitting the linecenter versus time then extrapolating to zero interrogation time. One interesting result is that for resonantly enhanced two-photon transitions the comb mode connecting the  $5S_{1/2}F = 2 \rightarrow 5P_{3/2}F = 3$  transition can be either resonant, blue detuned, or red detuned. By detuning the comb from exact intermediate resonance the heating rate is greatly reduced (Marian et al., 2004).

Another systematic error commonly encountered in two-photon transitions is the AC Stark shift due to off-resonant intermediate states. Again in this case focus is placed on the  $5S_{1/2}F = 2 \rightarrow 5P_{3/2}F = 3 \rightarrow 5D_{5/2}F = 4$  transition which is somewhat simplified because transitions to the final state are only allowed via the  $5P_{3/2}F = 3$  intermediate state due to hyperfine selection rules. A measurement of the  $5D_{5/2}F = 4$  linecenter versus time, shown in Fig. 11, illustrates the positive or negative Stark shift as a function of detuning from the intermediate state. This emphasizes the importance of being exactly on resonance with the intermediate state when conducting highly accurate spectroscopy, but also that if the comb is made exactly resonant the Stark shift is reduced. Furthermore it should be men-

tioned that, due to the regular spacing of modes, when one mode is resonant with the intermediate state then for every mode detuned to the red of the intermediate resonance there is one to the blue side with an equal detuning. To within limits due to the spectral shape of the pulse the Stark shifts from off resonant modes tends to cancel out, regardless of the spectral phases of the individual modes.

### 3.3.2. Multi-Photon DFCS of Cesium

As discussed in Section 3.3, two-photon spectroscopy is greatly enhanced in the case where the two-photons are resonant with an intermediate state. While this enhancement can be accomplished using the two degrees of frequency control available with the comb as discussed above, it is also possible to utilize the motion of the atoms to eliminate the need to fine tune both the carrier-envelope offset frequency and the repetition rate. This Doppler-induced enhancement was demonstrated in the work of Mbele et al. (in preparation).

In that work, two-photon spectroscopy was performed on four different excited states in Cs. A schematic of the experimental setup is shown in Fig. 12(a). The Cs was contained in a vapor cell at room temperature, resulting in a velocity distribution with an average velocity of  $v = 190$  m/s. The output of the frequency comb was split and the two beams were counter-propagated through the vapor cell. The frequency comb was derived from an octave-spanning mode-locked Ti:sapphire laser with a  $\approx 1$  GHz repetition rate (Fortier et al., 2006a). The carrier-envelope offset frequency was stabilized using the  $f$ -to- $2f$  technique described in Section 2.1. The repetition rate was stabilized to a synthesizer referenced to an H maser. The repetition rate of the synthesizer was scanned and fluorescence from the  $7p^2P \rightarrow 6s^2S_{1/2}$  transition was detected with a photomultiplier tube, see Fig. 5(b). The resulting spectrum is shown in the upper plot of Fig. 12(b). The different peaks are a result of different hyperfine transitions between the ground state and four excited states: the  $8s^2S_{1/2}$ ,  $9s^2S_{1/2}$ ,  $7d^2D_{3/2}$ , and  $7d^2D_{5/2}$ . By filtering the different optical beams, it was possible to isolate and identify the peaks and make precision measurements of the two-photon transition frequencies.

Each of the peaks is a result of an enhancement of a single pair of comb modes resonant with both stages of the excitation, similar to the enhancement observed by Weber and Sansonetti (1987). Because of the large velocity distribution, there are atoms which are Doppler shifted into resonance with the first stage of the excitation regardless of the repetition rate and carrier-envelope offset frequency. For specific repetition rates, these Doppler shifted atoms will also be resonant with the second stage of the excitation. By considering the velocity groups resonant with each stage of the excitation it can be shown that both of the two comb modes are resonant when the repetition rate is

$$f_r = \frac{2v_{1,0}v_{2,0} - f_o(v_{1,0} + v_{2,0})}{n_1v_{2,0} + n_2v_{1,0}}, \quad (3)$$

were  $\nu_{1,0}$  and  $\nu_{2,0}$  are the Doppler-free frequencies of the first and second stages of excitation, respectively, of the two-photon transition. This eliminates the need for independent adjustment of the carrier-envelope offset frequency in order to achieve the double resonance condition. Because the velocity class that is excited depends on the frequency of both stages of the two-photon excitation, the spectrum also provides information concerning the intermediate state frequency.

The velocity selective enhancement selects out a single pair of comb modes. Consequently, one can consider the excitation of a given state as equivalent to the excitation by two cw lasers. The middle trace in Fig. 12(b) shows the

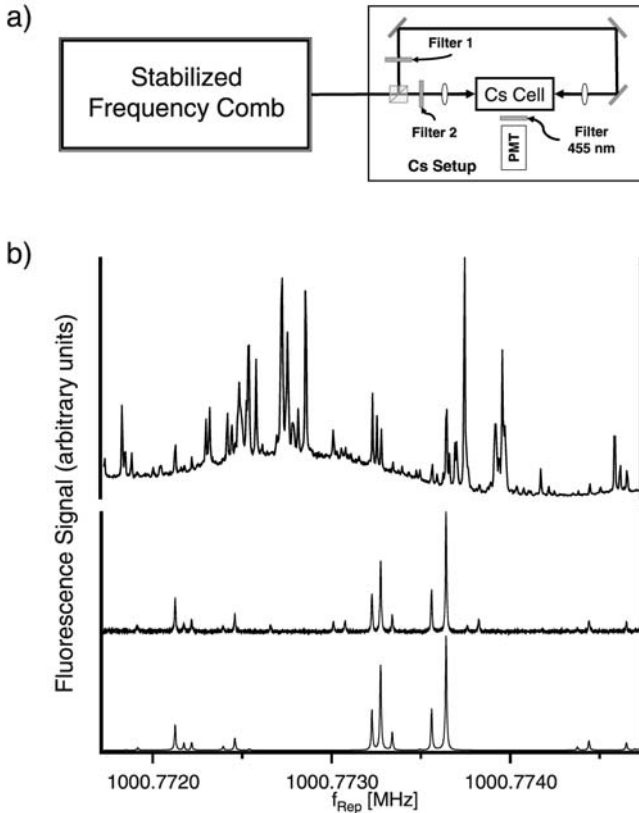


FIG. 12. Two-photon excitation of Cs states. (a) shows a block diagram of the experiment. The top trace in (b) shows the spectrum obtained with an unfiltered comb. Four different excited states are present. The middle trace in (b) shows the spectrum obtained by filtering the comb so that only the  $6s^2S_{1/2} \rightarrow 6p^2P_{3/2} \rightarrow 8s^2S_{1/2}$  transition contributes. The bottom trace shows the calculated spectrum.

experimental spectrum acquired by filtering the two arms to observe only the  $6s^2S_{1/2} \rightarrow 9s^2S_{1/2}$  transition through the  $6p^2P_{3/2}$  intermediate state. Below it is the calculated spectrum generated by integrating the two-photon formula, Eq. (1), over the velocity distribution. It is possible to determine the frequency of the transitions, as well as the hyperfine constants of the states, by calculating spectra with different transition frequencies and hyperfine constants and matching the calculations to the experimental spectra. In the experiment of Mbele et al. (in preparation), the frequencies and hyperfine coefficients of the states were determined with an accuracy of 50–200 kHz.

### 3.4. SHORT WAVELENGTH DFCS

One of the most promising future applications of DFCS is to truly take advantage of the phase coherence of the comb combined with the efficient nonlinear conversion enabled by high peak intensities. Already some experiments have been conducted by frequency mixing the fs pulses to shorter wavelengths where cw lasers are not easily accessible. There are two experiments conducted to date utilizing multi-pulse quantum interference for spectroscopy in the VUV spectrum. The first demonstration of this technique used two-photon absorption at 212 nm in krypton by pairs of phase coherent pulses (Witte et al., 2005). The most recent

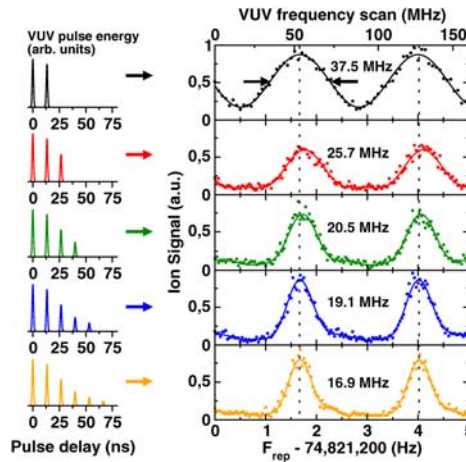


FIG. 13. Measured xenon ion yield versus  $f_r$  for 2, 3, 4, 5, 6 pulses. The strength of the pulses decreases versus pulse number as the amplifier inversion decays. These results emphasize several aspects of DFCS. The signal linewidth reduces versus the number of pulses used, note it is sinusoidal for two pulses similar to Ramsey spectroscopy. Secondly, the single resonant line repeats periodically due to the comb structure of the laser. [Reprinted with permission from Zinkstok et al. (2006).]

example demonstrates multi-pulse DFCS of the  $5p^6\ ^1S_0 \rightarrow 5p^5\ (^2P_{3/2})5d[\frac{1}{2}]_1$  transition in xenon at 125 nm, see Zinkstok et al. (2006). Pulses from a Rb-atomic-clock-referenced Ti:sapphire frequency comb are injected into a multipass Ti:sapphire amplifier that outputs pulses of about 25  $\mu$ J centered at 750 nm with a 0.7 nm spectral width. From two to six pulses may be injected into the amplifier then frequency doubled in BBO and subsequently tripled in either oxygen or krypton. The resulting pulses are phase coherent and have an energy of 50 fJ. These pulses are used to coherently excite xenon atoms in an atomic beam of <10 MHz Doppler width. The excited atoms are then ionized by a second pulse and the ions are detected. Using this technique the authors were able to scan  $f_r$  and recover a transition linewidth as narrow as 7.5 MHz FWHM. Shown in Fig. 13 is the ion signal in arbitrary units versus the  $f_r$  detuning from the mean value for excitation by two to six VUV pulses.

#### 4. Multi-Frequency Parallel Spectroscopy

In most DFCS experiments, the atomic system under study has acted as the high-resolution spectral discriminator that effectively selects an individual frequency comb element (or groups of comb elements) out of a greater number of elements that passed through the sample. The interaction of the optical frequency comb with the atomic system is then detected by the fluorescence or ionization from an excited state. A different approach involves the use of a high-resolution spectrometer to spectrally resolve individual comb elements in a parallel architecture. This allows a multi-channel detector to subsequently measure the amplitude (and potentially the relative phase—with appropriate reference) of the comb elements.

The challenge of resolving individual comb modes arises from the combined density and bandwidth of a typical optical frequency comb. A Fabry–Perot etalon has sufficient finesse to easily resolve the individual modes of a frequency comb with mode spacing below 100 MHz; however, the free spectral range of such an etalon does not typically exceed 100 GHz, which limits the bandwidth over which it can be used. On the other hand, grating-based spectrometers of reasonable size and cost can cover hundreds of THz, but the typical resolution does not exceed 10 GHz, which is insufficient to isolate individual modes of most femtosecond frequency combs. Such conflicting requirements of high resolution over large bandwidths are not necessarily new to the field of optics, and one solution involves using two spectrally dispersive elements (e.g. an etalon and a grating) along orthogonal spatial dimensions (Jenkins and White, 1976). An efficient implementation of this idea, originally directed toward separating densely-spaced optical communications channels (Xiao and Weiner, 2004; Wang et al., 2005) employs a diffraction grating orthogonal to a virtually-imaged phased array (VIPA) disperser (Shirasaki, 1996), which is essentially a variation

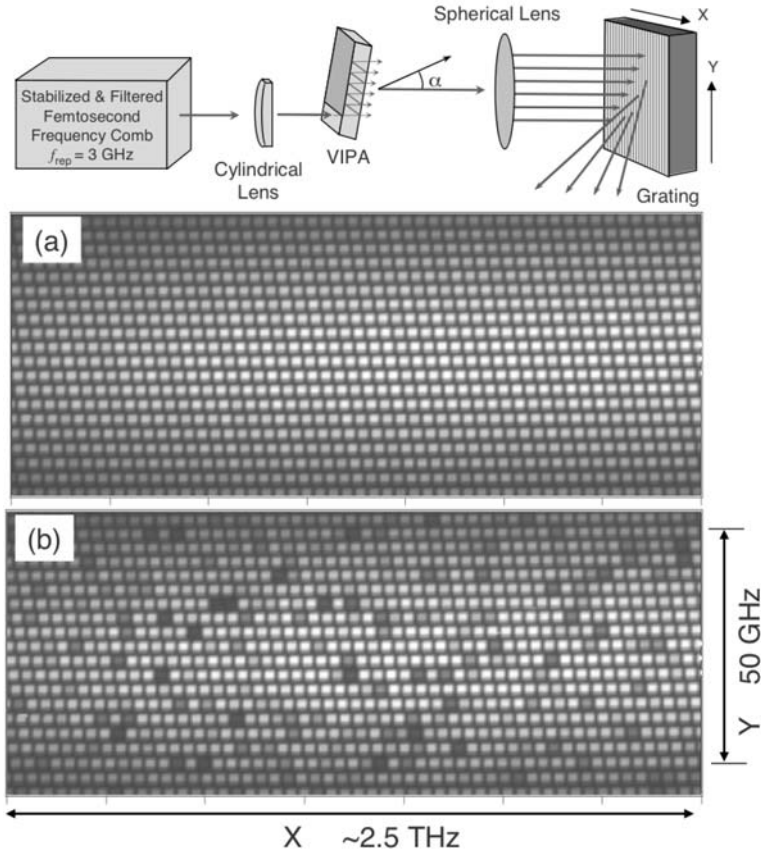


FIG. 14. A high resolution virtually-imaged phased array (VIPA) disperser is used in combination with a lower resolution diffraction grating to spatially resolve the filtered frequency comb of a frequency-stabilized, broadband Ti:sapphire femtosecond laser. (a) The spectrometer output in the region of 633 nm, as measured on a CCD element, consists of a 2-d array of the frequency comb modes, where each dot of this image represents an individual mode. Within a column (Y), which is tilted by the grating dispersion, the dots are separated by the mode spacing (3 GHz in this case). Within each row (X), the dots are separated by the VIPA free spectral range (FSR 50 GHz in this case). (b) Same frame as above, but now with iodine cell present. Note that some modes are missing or noticeably attenuated due to the presence of the iodine.

on the well-known plane-parallel etalon. In this case, the grating should provide spectral resolution better than that of the VIPA's free spectral range (FSR).

A high-resolution spectrometer designed for resolving individual comb modes is diagrammed in Fig. 14 (Diddams et al., 2006). The VIPA is a plane-parallel solid glass etalon, where the input beam is focused to a line and injected at an

angle through an uncoated entrance window on the etalon's front face. The remainder of the front face is coated with a high-reflective dielectric, while the back face has a dielectric coating with 96% reflectivity. The multiple reflections within the VIPA etalon interfere in such a way that the exiting beam has its different frequencies emerging at different angles. In this case, the VIPA has a free spectral range of 50 GHz, determined by its thickness and index of refraction. The 2400 line/mm grating, used at a large angle of incidence and oriented with its dispersive axis orthogonal to that of the VIPA, provides 20 GHz spectral resolution that is sufficient to separate the various orders of the VIPA etalon.

The output of the VIPA/grating spectrometer is imaged onto a CCD camera, resulting in the array of dots, representing the individual comb modes, see Fig. 14(a). In this example, a frequency comb with elements spaced by 3 GHz was created by filtering the 1 GHz comb produced by a broad bandwidth Ti:sapphire laser. Approximately 2200 individual modes have been resolved within a 6.5 THz bandwidth captured in a few millisecond exposure on the CCD, for clarity the bandwidth is restricted to 2.5 THz in Fig. 14. In the vertical direction of this image, the data repeats every 50 GHz (at the VIPA FSR), and adjacent columns are also separated by the FSR of the VIPA. Full details on the indexing and counting of the numerous modes, as well as the frequency calibration are described in a recent publication (Diddams et al., 2007). The repetitive nature of the data is evident in Fig. 14(b), which is an image acquired with the iodine vapor cell inserted in the beam path. The cell is at room temperature and multi-passed to yield an equivalent length of 2 m. As clearly seen, numerous modes which coincide with absorption features of iodine are attenuated. Given the particular phase-locked values of  $f_o$  and  $f_r$ , the absolute frequency of each mode (or equivalently each CCD pixel) can be determined, thus providing a rapid means of identifying atomic or molecular species. While the VIPA spectrometer resolution is presently 1.2 GHz (at 475 THz), spectroscopic features down to the linewidth of the comb lines can be distinguished. Scanning the repetition rate or offset frequency of the laser enables one to scan out the full optical spectrum with a resolution suitable for the system under study (Diddams et al., 2007).

#### 4.1. CAVITY ENHANCED DFCS

With every optical comb component efficiently coupled into a respective high-finesse cavity mode, one can establish a network of parallel channels for ultra-sensitive detection of molecular dynamics and trace analysis. This configuration provides an ideal spectroscopic paradigm suitable for the next generation of atomic and molecular measurements. The approach presents simultaneously the following attractive characteristics: (i) A large spectral bandwidth allowing for the observation of global energy level structure of many different atomic and molecular species; (ii) High spectral resolution for the identification and quantitative

analysis of individual spectral features; (iii) High sensitivity for detection of trace amounts of atoms or molecules and for recovery of weak spectral features; and (iv) A fast spectral acquisition time, which takes advantage of high sensitivity, for the study of dynamics.

The development of cavity-enhanced direct frequency comb spectroscopy utilizing a broad bandwidth optical frequency comb coherently coupled to a high-finesse optical cavity has been demonstrated (Thorpe et al., 2006, 2007). Hundreds of thousands of optical comb components, each coupled into a specific cavity mode, collectively provide sensitive intracavity absorption information simultaneously across a 100 nm bandwidth in the visible and near IR spectral region. By placing various atomic and molecular species inside the cavity, real-time, quantitative measurements of the trace presence, transition strengths and linewidths, and population redistributions due to collisions and temperature changes have been demonstrated. This novel capability to sensitively and quantitatively monitor multi-species molecular spectra over a large optical bandwidth in real-time provides a new spectroscopic paradigm for studying molecular vibrational dynamics, chemical reactions, and trace analysis. The continuing development of state-of-the-art laser sources in the infrared spectral regions, possibly even covering the important 3  $\mu\text{m}$  area, will further improve the system's sensitivity.

The use of cavity enhancement allows for the measurement of optical absorption with sensitivities that are many orders of magnitude higher than what can be achieved with single pass absorption measurements. Cavity enhancement is most easily understood as an increased interaction length between the probe light and an intracavity absorber. Once coupled into the cavity, a photon will on average traverse the cavity a number of times that is proportional to the inverse of the mirror losses before decaying out of the cavity. Since the mirror losses can be made very small (as low as 10 parts per million) the enhancement in the light/matter interaction length can be more than 100,000. Because of its high sensitivity, cavity enhancement is useful when investigating atomic and molecular systems that have weak oscillator strengths, or in cases where only a trace amount of the target atom or molecule is present.

In the mid to late eighties the effect of cavity enhancement led to the development of cavity ring-down spectroscopy (CRDS), see for example Anderson et al. (1984), O'Keefe and Deacon (1988). CRDS has the useful feature that the laser intensity is removed from the measurement of optical absorption. Instead, the beam incident on the cavity is turned off and the rate of photon decay out of the cavity is measured. In this way, laser intensity fluctuations and noise associated with coupling the laser to the optical cavity do not affect the absorption measurement. By the mid to late nineties, CRDS was being used in a wide variety of applications and had achieved fantastic detection sensitivities, for example  $3 \times 10^{-12}/\text{cm}$  at 1 s integration time (Ye and Hall, 2000) or using the more complicated but sensitive technique, NICE-OHMS,  $2 \times 10^{-14}/\text{cm}$  at 1 s is possible (Ye et al., 1998).

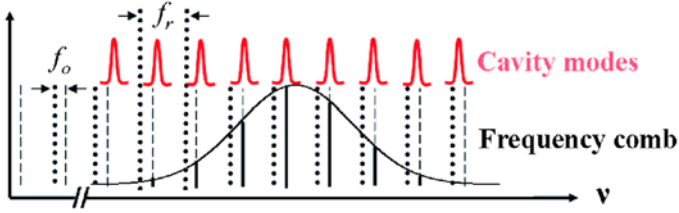


FIG. 15. When the frequencies of an optical frequency comb are made to overlap with the resonant modes of a high-finesse optical cavity, >90% of the broadband light can be coupled into the cavity. Nonuniform cavity mode spacing caused by dispersion limits the spectral bandwidth that can be coupled into the cavity.

Over the past decade, applications that require large spectral bandwidths such as the simultaneous detection of many different molecular species have led to the development of cavity enhanced systems based on mode-locked lasers (Crosson et al., 1999; Gherman et al., 2004; Thorpe et al., 2006). Using mode-locked lasers, broadband light can be coupled into a high-finesse optical cavity with very high efficiency, see Fig. 15. As a result, low average powers can be used to perform spectroscopy over a large spectral bandwidth. Also, the high peak intensities produced by ultrashort pulses are convenient for frequency conversion and spectral broadening such that modern mode-locked lasers can access any spectral region from the extreme ultraviolet to the far infrared and provide large spectral bandwidths for investigation and detection of a wide variety of atomic and molecular species (Dudley et al., 2006; Jones et al., 2005). In addition, massively parallel detection schemes have enabled the acquisition of broadband and high resolution atomic and molecular spectra in sub-millisecond timescales (Scherer et al., 2001; Diddams et al., 2007).

Efficient coupling of an optical frequency comb into a high-finesse optical cavity requires independent control of both the repetition frequency ( $f_r$ ) and carrier offset frequency ( $f_o$ ) of the comb. Using these controls the comb modes can be appropriately spaced and shifted to overlap the cavity modes (Jones and Ye, 2002). The bandwidth of the incident comb that can be coupled into the cavity is a function of the cavity dispersion and finesse. Cavity dispersion makes the resonant modes of the cavity have a nonuniform spacing as shown in Fig. 15 (Thorpe et al., 2005). Specifically, the frequency-dependent free spectral range (FSR) of the cavity is given by:

$$\text{FSR}(\omega) = \frac{c}{2L + c \left. \frac{\partial \phi}{\partial \omega} \right|_{\omega_0}}. \quad (4)$$

Here  $c$  is the speed of light,  $L$  is the cavity length, and  $\phi$  is the frequency-dependent phase shift due to reflections from cavity mirrors and the intracavity

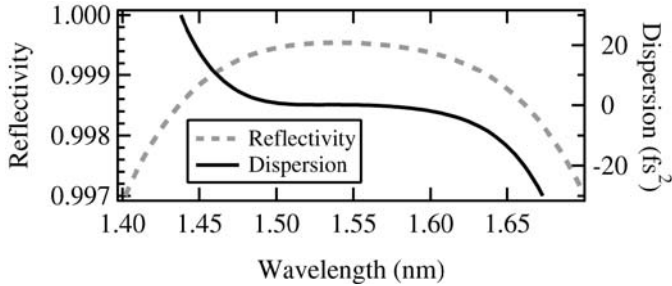


FIG. 16. The reflectivity and dispersion curves of Bragg reflectors constructed from alternating layers of silicon dioxide and niobium oxide centered at 1550 nm.

medium. The cavity finesse determines the linewidth of the cavity modes according to the relationship  $\Delta\nu = \text{FSR}/\mathcal{F}$  where  $\mathcal{F}$  is the cavity finesse and  $\Delta\nu$  is the cavity linewidth. For a high-finesse optical cavity constructed from two identical mirrors the finesse can be approximated by  $\mathcal{F} \approx \pi/(1-R)$  where  $R$  is the reflectivity of the cavity mirrors. The spectral bandwidth that can be coupled into the optical cavity can be found by evaluating the walk-off integral:

$$\Delta\nu = \frac{\text{FSR}(\omega)}{\mathcal{F}} = \frac{1}{\pi} \int_0^{\omega_{1/2}} \left( \frac{\text{FSR}(\omega)}{f_r} - 1 \right) d\omega. \quad (5)$$

Here the spectral bandwidth coupled into the cavity is  $2\omega_{1/2}$ . The walk-off integral illustrates the tradeoff between the cavity finesse and the coupled spectral bandwidth. As the finesse increases (leading to increased sensitivity) the bandwidth coupled into the cavity decreases. The typical dispersion and reflectivity curves for Bragg reflectors used to construct broadband enhancement cavities are shown in Fig. 16. If the comb is locked to the cavity modes, coupled bandwidths of 30 to 60 nm at 1550 nm (limited by the dispersion and reflectivity of the mirrors) are typical. For broader bandwidth measurements, the comb can be dithered over the cavity modes. Using this method, the measurement bandwidth is only limited by reflectivity of the cavity mirrors (typically 200 nm at 1550 nm), however, the measurement rate or duty cycle is reduced by the dither.

Using techniques of spectral broadening, optical frequency combs can have a very broad spectrum allowing a single laser source to perform spectroscopy over more than an octave of spectrum. A modest example of a spectrum that can be generated using highly nonlinear fiber is shown in Fig. 17. Because of this, it is typically the cavity mirrors that limit the spectral bandwidth of cavity enhanced measurement systems. However, the continued development of broad-band, high reflectivity, and low-loss mirror coatings as well as the recent development of

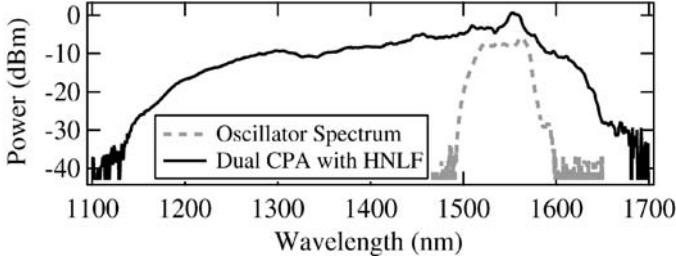


FIG. 17. The spectrum of an  $\text{Er}^{+3}$  mode-locked fiber laser before and after amplification and spectral broadening via highly nonlinear fiber. Both spectra were recorded with 1 nm resolution.

broad-band, high-finesse prism cavities will relax this limitation in future systems.

A number of parallel detection techniques have been developed to simultaneously read-out the many parallel channels that are available in cavity transmission. The simplest form of parallel detection uses a direct absorption measurement. Here, the light transmitted from the cavity is spectrally dispersed and the intensity is recorded at different spectral regions with a CCD or a diode array. The transmitted beam can be spectrally resolved with either a grating spectrometer producing a 1-dimensional dispersion pattern or with a virtually-imaged phased array (VIPA) spectrometer that provides a higher resolution and more compact 2-dimensional dispersion pattern (Diddams et al., 2007). To simultaneously record multiple ring-down signals requires some more complicated techniques. One clever way to do this involves the use of a rotating mirror to convert the time-domain information contained in the ring-down signal into a spatial position of the beam on a CCD chip (Scherer et al., 2001).

A typical frequency comb based cavity ring-down system shown in Fig. 18 consists of a mode-locked laser, a high-finesse optical cavity, a broadband detection scheme, and feedback to maintain the comb and cavity in resonance.

The inset in Fig. 18 describes the basic requirements for coupling the comb to the cavity. First, the FSR of the cavity must be equal to the laser  $f_r$ . Next,  $f_o$  must be set such that the comb frequencies are shifted to overlap the cavity modes. Once light is built-up into the cavity, an optical switch is used to turn off the light incident on the cavity at which time the photons in each cavity mode decay out of the cavity with a characteristic time constant that depends on the cavity length and the total cavity losses,

$$\tau = \frac{1}{\text{FSR}(\omega)\text{Loss}} = \frac{1}{\text{FSR}(\omega)(1 - R_1 R_2 e^{-2\alpha(\omega)L})}. \quad (6)$$

Here,  $R_1$  and  $R_2$  are the reflectivities of the cavity mirrors,  $L$  is the cavity length, and  $\alpha(\omega)$  is the frequency-dependent intracavity absorption. The light that decays

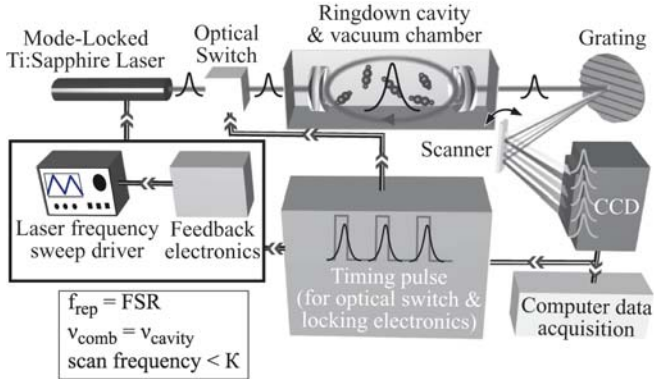


FIG. 18. Schematic of broadband cavity ring-down spectroscopy. The inset box lists the basic requirements for coupling the frequency comb to the cavity and the maximum rate that cavity enhanced measurements can be made, where  $\kappa = \frac{1}{\tau}$ .

from the cavity is spectrally dispersed with a grating. The decay rate is measured by sweeping the dispersed beam across a CCD chip with a rotating mirror (Scherer et al., 2001). In this system, the comb is dithered over the cavity modes such that the cavity builds-up and rings-down twice per modulation cycle. The feedback scheme that keeps the comb resonant with the cavity modes typically consists of two low speed servos. The first servo has a bandwidth of 10 Hz and maintains the cavity transmission peak at the center of the  $f_r$  dither by actuating  $f_r$ . The second servo actuates  $f_o$  via the laser pump power or by rotating a dispersive element inside the laser cavity to maximize the height of the cavity transmission peak.

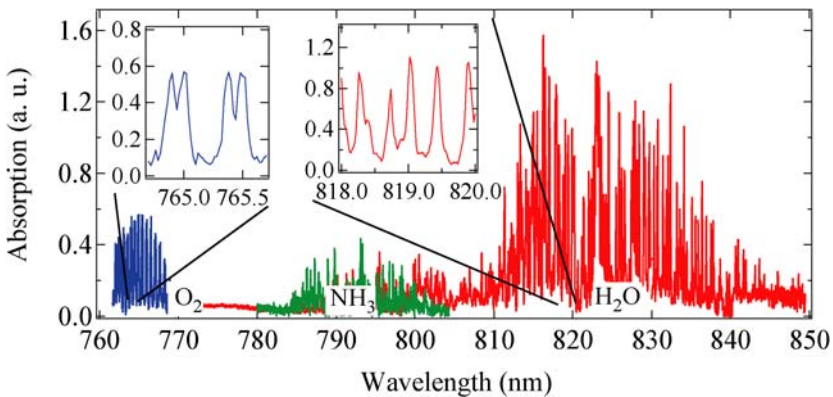


FIG. 19. The spectra of  $\text{O}_2$ ,  $\text{NH}_3$  and  $\text{C}_2\text{H}_2$  near 800 nm.

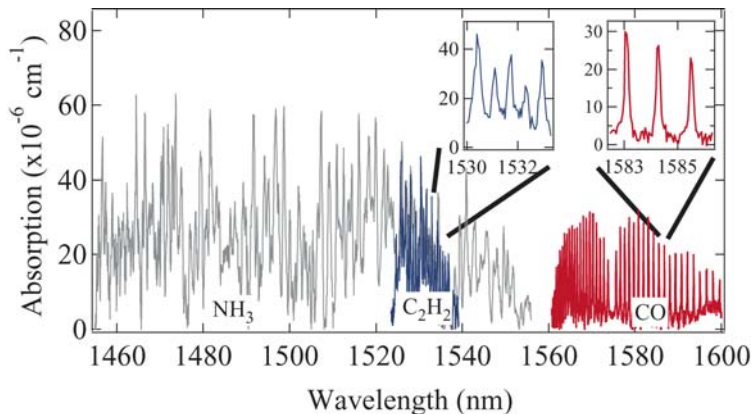


FIG. 20. The spectra of CO, NH<sub>3</sub> and C<sub>2</sub>H<sub>2</sub> near 1550 nm.

Recently, two systems have been constructed to demonstrate CRDS based on an optical frequency comb (Thorpe et al., 2006, 2007). The first of these systems was based on a mode-locked Ti:sapphire laser with a 100 nm spectral bandwidth centered at 800 nm. Figure 19 shows the spectra of O<sub>2</sub>, NH<sub>3</sub>, and H<sub>2</sub>O recorded with the Ti:sapphire comb-based CRDS system. The ring-down cavity used for these measurements was a two mirror linear cavity with mirror reflectivity  $R = 0.9993$  and a FSR of 200 MHz.

The second frequency comb CRDS system was based on a mode-locked erbium-doped fiber laser. Figure 20 shows the spectra of NH<sub>3</sub>, C<sub>2</sub>H<sub>2</sub>, and CO recorded with the erbium fiber laser CRDS system. The ring-down cavity used for these measurements was a two mirror linear cavity with mirror reflectivity  $R = 0.9996$  and a FSR of 100 MHz.

## 5. Coherent Control Applications

Direct frequency comb spectroscopy has also been applied to conduct coherent control experiments at vastly enhanced spectral resolution. A basic feature of coherent control is the manipulation of the final state of a system by controlling quantum interference routes. In contemporary coherent quantum control, short pulses are commonly used due to their broad spectrum and known, stable spectral phase. Shaping the spectrum and the spectral phase of the pulse allows control over the interference between different quantum paths, steering an interaction toward a desired outcome. The main improvement offered by the frequency comb is that it allows for the coherent interaction time to be much longer than the duration of a single (shaped) pulse. Due to the inter-pulse coherence enabled by a

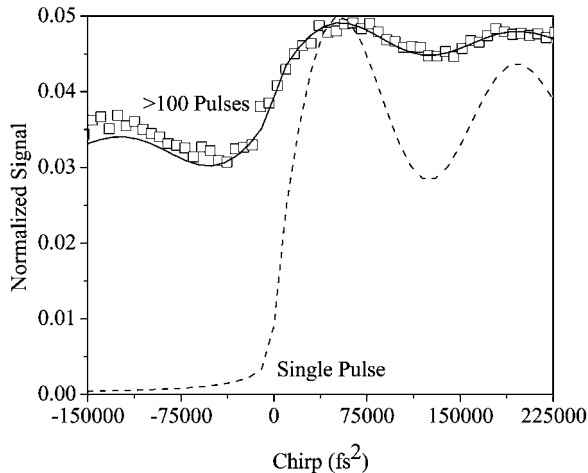


FIG. 21. The measured  $5D_{5/2}F = 4$   $^{87}\text{Rb}$  fluorescence is shown (squares) versus chirp for steady state excitation. The solid line indicates the theory prediction at steady-state and the dashed line is for single-pulse excitation.

phase-stabilized frequency comb, it is possible to use the entire train for a coherent control process.

### 5.1. HIGH RESOLUTION COHERENT CONTROL

Some of the pioneering work on coherent control introduced either linear frequency chirp or discrete phase steps in a pulse spectrum to manipulate two-photon absorption in Alkali atoms such as  $^{87}\text{Rb}$ , see for example [Balling et al. \(1994\)](#), [Chatel et al. \(2003\)](#), [Meshulach and Silberberg \(1998\)](#). These experiments were conducted with only one pulse, therefore the resolution was significantly lower than allowed by DFCS. The experiment presented in [Stowe et al. \(2006\)](#) extends some of the pioneering work on coherent control to high resolution by introducing linear frequency chirp to a coherent pulse train, or in other words adjusting the phase of the comb modes used in DFCS. In this experiment a grating based pulse stretcher/compressor was used to introduce up to  $\pm 225000 \text{ fs}^2$  of dispersion to the pulses before they excite the  $5S_{1/2}F = 2 \rightarrow 5P_{3/2}F = 3 \rightarrow 5D_{5/2}F = 4$  transition in  $^{87}\text{Rb}$ . [Figure 21](#) shows the measured 5D population versus the pulse chirp. Particularly interesting is that the difference in signal between positive and negative chirp decreases significantly between single and multi-pulse experiments. In the single pulse case negative chirp excites essentially no population due to the fact the wavelength connecting the  $5S_{1/2}F = 2 \rightarrow 5P_{3/2}F = 3$  transition arrives after the  $5P_{3/2}F = 3 \rightarrow 5D_{5/2}F = 4$  wavelength, essentially the time ordering

is wrong to complete a two-photon transition via the intermediate state. However, for multiple pulsed excitation the coherence between the atomic states excited by the first pulse remains intact for the second pulse, which can complete the two-photon transition. This is a clear example of an important difference between single and multiple shaped pulse excitation of an atomic or molecular system exhibiting a coherence time longer than the inter-pulse period. Several previous papers (Balling et al., 1994; Chatel et al., 2004, 2003) have demonstrated and modeled the oscillation of the excited  $5D$  population versus chirp. The period of this oscillation is inversely proportional to the detuning of the intermediate state from half the two-photon transition frequency, for example 1 THz for  $5P_{3/2}$  and 8 THz for  $5P_{1/2}$ . Unlike previous single pulse coherent control experiments the high resolution enabled by the comb can be used to control the population transfer to a single excited hyperfine level,  $5D_{5/2}F = 4$ . Furthermore, due to hyperfine selection rules, this level may only be reached from a single intermediate state,  $5P_{3/2}F = 3$ . For this reason the measurement shown in Fig. 21 and the observed oscillation period versus chirp can be attributed to only one intermediate state, as opposed to all the states within the  $5P$  manifold. This demonstrates that DFCS can extend some classic single pulse coherent control experiments, limited to THz order resolution, to natural linewidth limited resolutions. Coherent control experiments utilizing DFCS can now truly control the population transfer to a single quantum state.

## 5.2. EXTENSION OF DFCS TO STRONG FIELD COHERENT CONTROL

While analysis of coherent quantum control is relatively simple in the weak field perturbative domain (Shapiro and Brumer, 1986, 2003a, 2003b; Tannor and Rice, 1985; Rice and Zhao, 2000), extension to strong fields is not straightforward. Analytic models exist only for simple cases (Vitanov et al., 2001; Gaubatz et al., 1990; Dudovich et al., 2005; Lee et al., 2004) and solutions are often found by numerical optimizations (Rabitz et al., 2000). Here, the concept of coherent accumulation of a train of pulses also proves very useful. While at first, the need to consider the effect of the whole pulse train seems to further complicate the analysis, it can in fact considerably simplify the design. Specifically, since each pulse in the train achieves only a fraction of the overall population transfer, one can exploit analytic perturbative models to design “ideal” weak pulses, relying on the coherent accumulation of all pulses to achieve the high overall efficiency. This avoids the complication of strong field design while gaining the high spectral selectivity offered by the frequency comb.

As a model problem to illustrate the concept of *strong-field* control with the comb, we discuss a narrow-band Raman transition between molecular vibrational levels from a single vibrational level embedded in a dense environment of other

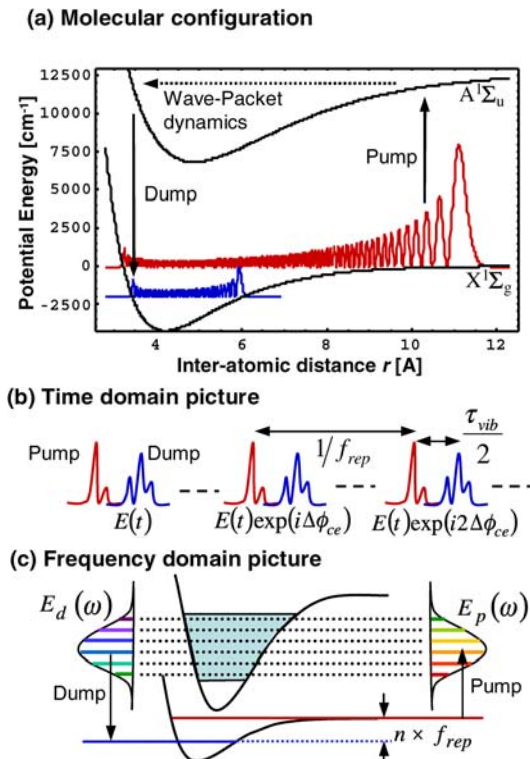


FIG. 22. Basic Raman control scheme. (a) Typical electronic potentials and vibrational levels (here, Morse potential fits of  $Rb_2$ ). Population is transferred from the input vibrational level near the dissociation limit ( $v' = 130$ ) to a deeply bound level ( $v = 45$ ), mediated via a broadband wave-packet in the excited electronic potential. (b) Time-domain picture. A train of phase coherent pump–dump pulse pairs interacts with the molecule. Pulse pairs are shaped to achieve efficient population transfer. The intrapair time is half the vibration time ( $\tau_{vib}$ ) of the intermediate wave-packet and the inter-pair time is the repetition time of the source  $1/f_r$ . (c) Frequency-domain picture. A tooth-to-tooth match between the pump and the dump frequency combs, with  $f_r$  equal to a sub-harmonic of the net Raman energy difference, locks the relative phase between pulse pairs to the free evolving Raman phase.

levels near the dissociation limit, to a single deeply bound vibrational level, as shown in Fig. 22, Pe'er et al. (2007). Each pump–dump pulse pair in the coherent train of shaped pulse pairs is weak, i.e., it transfers only a small fraction of the input population to the target state and only coherent accumulation of many pulses enables a high overall transfer efficiency. In the time domain, each pump pulse excites a wave-packet that starts to oscillate in the excited electronic potential. After half a vibration, this wave-packet reaches the inner turning point where the dump pulse drives it to the target state. Since population appears on

the excited potential only for half a vibration, this scheme eliminates spontaneous emission losses. In order to enable coherent accumulation of population at the target state, the temporal phase difference between pulse pairs should match the phase of the free evolving Raman coherence. In the frequency domain, the combs of the pump and the dump pulses must overlap tooth to tooth and the repetition rate  $f_r$  must match a sub-harmonic of the Raman energy difference, as illustrated in Fig. 22(c).

The coherent accumulation process gradually transfers the population from the input to the target state. A weak pump pulse can indeed excite a small fraction of population from the input state, but the very first dump pulse must have a “pulse area” near  $\pi$  to drive all this population to the *empty* target state. The second dump pulse, however should have an “area” of only  $\pi/2$ , because now the excited population is about equal to the population already in the target state from the previous dump, just like in a Ramsey experiment. Similarly, as the input state is depleted, the pump “area” should slowly increase to excite the same population every time, reaching  $\sim\pi$  for the very last pump pulse. In general, the fraction of population excited (or dumped) by a pulse of “area”  $A$  is  $\sin^2(A/2)$ . As population is accumulated in the target state and depleted from the input state, the dump “area” of the  $n$ th pulse  $A_d[n]$  should decrease and the pump “area”  $A_p[n]$  increase according to

$$\sin^2\left(\frac{A_d[n]}{2}\right) = \frac{1}{n}, \quad \sin^2\left(\frac{A_p[n]}{2}\right) = \frac{1}{N - n + 1}, \quad (7)$$

for each pulse pair to transfer the same fraction of population (total of  $N$  pulses). Another equally valid solution is to fix the pump area and vary the dump according to the evolving population distribution. In general, for any given pump series, a dump series can be matched according to the  $n$ th fraction of excited population. Clearly the very first dump pulses and the last pump pulses are of areas near  $\pi$  and cannot be considered weak, but for a large  $N$ , the majority of the population is transferred by the accumulative effect of all pulses, which are mostly weak. Consequently, even if the first (last) pulses do not have the required area or are complicated by multi-photon effects, the overall process can remain efficient. Experimentally, current intensity modulators can easily meet the required pulse area variation for standard pulse repetition times of 1–10 ns.

For an efficient pump–dump process it is required that the wave-packet  $|\psi_p\rangle$ , excited by the pump from the input state  $|i\rangle$  and propagated for half a vibration, will overlap perfectly with the wave-packet  $|\psi_d^r\rangle$  that would have been excited from the target state  $|t\rangle$ , by the time-reversed dump. For weak pulses we can express these two wave-packets, using first order perturbation theory, as

$$|\psi_p\rangle \propto \sum_{\omega} E_p(\omega) e^{i\phi_D(\omega)} |\omega\rangle \langle\omega|d_e|i\rangle,$$

$$|\psi_d^r\rangle \propto \sum_{\omega} E_d^r(\omega)|\omega\rangle\langle\omega|d_{el}|t\rangle, \quad (8)$$

where  $|\omega\rangle$  denotes the vibrational states in the excited potential using the detuning  $\omega$  from the pulse carrier frequency as a vibrational index,  $F_p(\omega) = \langle\omega|d_{el}|i\rangle$  and  $F_d(\omega) = \langle\omega|d_{el}|t\rangle$  are the pump and the dump transition dipole matrix elements, which under the Condon approximation are proportional to the Franck–Condon factors  $\langle\omega|i\rangle$ ,  $\langle\omega|t\rangle$ .  $d_{el}$  is the electronic transition dipole moment and  $E_p(E_d^r)$  is the spectral amplitude of the pump (time-reversed dump) field.  $\phi_D(\omega)$  is the spectral phase acquired by the wave-packet between the pulses, which reflects both the delay of half a vibration and the dispersion of the wave-packet as it oscillates in the anharmonic excited potential. For a given molecular potential, both the dipole matrix elements and  $\phi_D(\omega)$  can be easily calculated.

As a result, perfect overlap of the two wave-packets can be achieved by shaping the pump field according to the dump dipole matrix elements and vice versa:

$$E_p(\omega) \propto F_d(\omega)A(\omega), \quad E_d(\omega) \propto F_p(\omega)A(\omega) \exp[i\phi_D(\omega)], \quad (9)$$

where  $A$  is an arbitrary spectral amplitude, common to both fields. Intuitively, this spectral shaping avoids pumping of what cannot be dumped (due to a node in the dump dipole matrix elements), and vice versa.

Within the perturbative discussion relevant to Eq. (9), the common spectral amplitude  $A(\omega)$  is completely arbitrary. Yet, it is desirable to minimize the total number of pulses for both practical reasons (accumulated phase noise) and fundamental ones (the total interaction time is limited by the coherence time of the input state), so one would probably prefer to use the strongest pulses that can still qualify as “weak”. The limiting power level is where two-photon (Raman) processes by a single pump or dump pulse become pronounced, and here common shaping will have an important effect. Specifically, in many cases of molecular dynamics, positively chirped (red to blue) excitation pulses can strongly suppress Raman processes that adversely affect the input wave-packet during the pulse (Bardeen et al., 1995; Cao et al., 1998; Malinovsky and Krause, 2001), leaving the excitation, although strong, essentially one-photon. Thus, chirping the pulses can improve considerably the dumping efficiency for the first dump pulse that is necessarily strong because it dumps to an empty target state. Common chirping can also help to resolve vibrational structure around the target state deep in the molecular well, yet it cannot resolve rotational/hyperfine structure, nor the dense environment around the input state. This is where the coherent accumulation proves powerful.

Representative simulation results of the full coherent accumulation process are shown in Fig. 23 for the interaction of a train of 40 pulse-pairs with the molecule. The pump pulses depleted  $>90\%$  of the input population, and when the inter-pulse phase was tuned to the Raman condition, 95% of this population reached the target

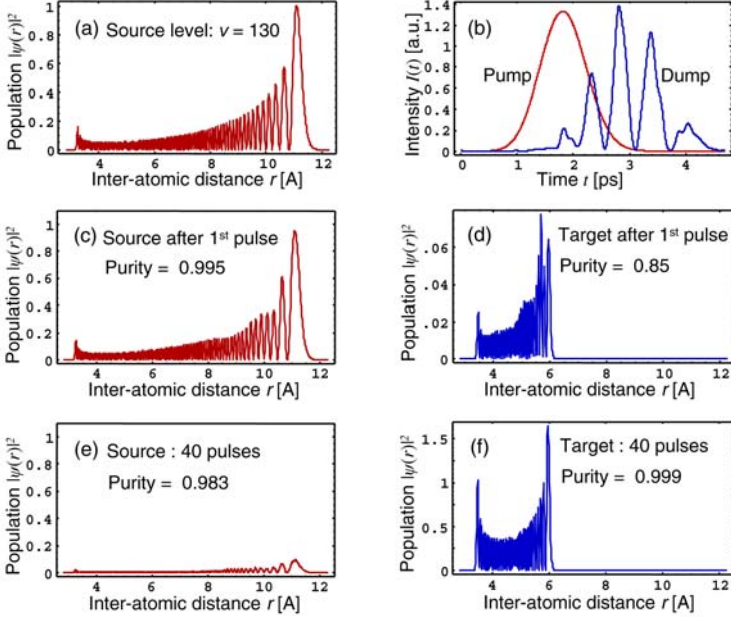


FIG. 23. Simulation results for the coherent accumulation process. The pump pulse power was fixed, exciting about 5.7% of the input population each time, and the dump area was varied to match with the accumulation progress. The pulses were  $\sim 10$  nm in bandwidth, chirped out to  $\sim 1.5$  ps by dispersion of  $500,000 \text{ fs}^2$ . (a) the input state population density, (b) the intensity temporal profile of the pulses (after strong chirp). (c) and (d) are the input and target wave-packet population densities after one pulse-pair, and (e) and (f) are the corresponding results after 40 pulses.

state. The purifying nature of the coherent accumulation process is demonstrated by the obtained final wave-packet—practically a single state.

The coherent accumulation proves to be quite robust against intensity fluctuations. Scaling the intensity of the pump or dump pulse train (or both) by a factor of two in simulation leaves the total transfer efficiency constant within a few percent. The exact variation of dump pulse area according to the accumulated population is also not critical. Even if the dump area is kept constant, the transfer efficiency is  $>50\%$  over a range of factor of two in intensity. The reason for this robustness is that even when not all population is dumped, the anharmonicity of the excited potential scrambles the lingering wave-packet between pulses, such that the interference with the next pumped wave-packet is neither constructive, nor destructive, but averages out (with background population decaying at  $1/f_r$  time scales). Therefore, pulse area errors do not coherently add from pulse to pulse.

To conclude, the presented scheme forms a unique and powerful combination of frequency-domain control (comb) and time-domain control (molecular dynam-

ics). As such, it enables performance of coherent control tasks with both high efficiency and unprecedented spectral resolution. Due to the use of weak pulses the process can be analyzed within a perturbative model, thus opening an analytic path to strong field problems that were so far accessible only by numerical optimizations.

## 6. Future Outlook

### 6.1. ATOMIC CLOCK APPLICATIONS

A general trend throughout the history of precision timekeeping has been to employ oscillators with an ever-increasing frequency, since a clock operating at a higher frequency provides greater precision through the finer sub-division of a unit of time. Following this trend over the past one hundred years, one finds the advance from pendulum clocks, to crystal quartz oscillators, to microwave atomic clocks, and now most recently, atomic clocks operating at optical and ultraviolet frequencies (Diddams et al., 2001; Ye et al., 2001). It is likely that this progression will continue in the future, and DFCS could play an important role in the push to still higher frequencies since the high peak powers of the associated femtosecond pulses provide an efficient means to generate coherent radiation at high frequencies. Some of the exciting new techniques for producing frequency combs in the extreme ultraviolet regime will be discussed in detail in the following section, but first we present a scheme of employing DFCS to control the frequency comb of a femtosecond laser, and thereby produce optical and microwave frequencies referenced directly to an atomic transition (Gerginov et al., 2005).

If the optical frequency  $\nu_n = f_o + n f_r$  of a certain comb component can probe, and then be directly stabilized to an atomic transition, the repetition rate instability will be given by  $\delta f_r / f_r = (1/n) \delta \nu_n / \nu_n$ , where  $\delta \nu_n / \nu_n$  is the optical frequency instability. In this way, an optical clock is realized without the use of cw lasers. The stability of the optical atomic reference is mapped onto the stability of  $f_r$ , which in turn can be measured and used as a frequency reference. Such an experiment has been realized by using the setup described in Section 3.2.2. The  $F = 3 \rightarrow F = 2$  transition of the Cs  $D_2$  line was excited using DFCS and the subsequent fluorescence was detected. By modulating  $f_r$  the fluorescence signal and its derivative shown in Fig. 24 were measured. The error signal was then used to steer  $f_r$  such that the specific optical mode ( $n = 352,210$ ) is frequency-locked to the center of the  $F_g = 3 - F_e = 2$  transition. Now atomically-stabilized, the stability of  $f_r$  was measured, and a fractional frequency instability plot are shown in Fig. 25. The plot shows that instability of better than  $10^{-11}$  can be easily achieved in 100 s integration time. While this example takes advantage of convenient, yet relatively broad near-infrared transition in cesium, the basic approach is one that could be applied to much higher (and narrower) frequency atomic transitions.

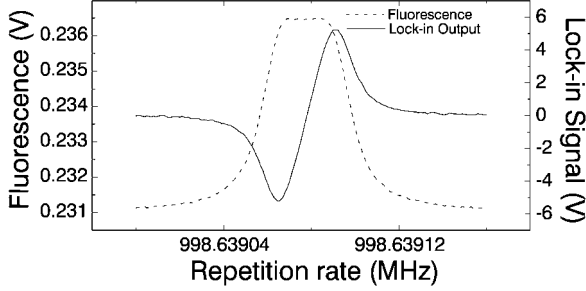


FIG. 24. Error signal used to lock the femtosecond laser repetition rate. A specific FLFC component excites  $F_g = 3 - F_e = 2$  transition of the Cs  $D_2$  line. The repetition rate was modulated at rate of 27 Hz with 15 Hz depth. Phase detection was used with 5 mV sensitivity and 1 s time constant.

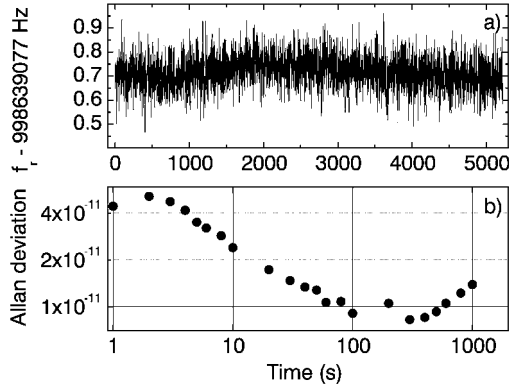


FIG. 25. Femtosecond laser repetition rate measured with  $n = 352,210$  optical component locked to  $F_g = 2 \rightarrow F_e = 2$  transition. The Allan variance calculated from the data is also shown.

## 6.2. XUV COMB DEVELOPMENT

While some of the powerful applications of the DFCS technique have been discussed in the previous sections, it is anticipated that its most powerful application is yet to come. Many scientific discoveries and technological advances are awaiting in the landscape of precision measurements and quantum control in the extreme ultraviolet (XUV) spectral region. With cw lasers unlikely to develop significantly into the XUV regime, DFCS is a uniquely attractive option for performing high resolution spectroscopy and quantum optics in the vast spectral region spanning from VUV to XUV.

To extend the coherent frequency comb structure and related precision measurement capabilities into the deep UV, recent research has focused on the demon-

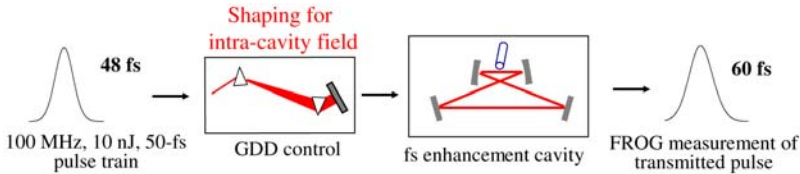


FIG. 26. Schematic setup of intracavity high-harmonic generation. The femtosecond pulse train, after proper dispersion compensation, is incident and stabilized to a high-finesse cavity of a bow-tie geometry, enhancing the pulse energy by nearly three orders of magnitude while maintaining a high repetition frequency inside the cavity. A gas target at the cavity focus enables phase-coherent high-harmonic generation, resulting in a phase-stable frequency comb in the VUV spectral region. Measurement of the pulse shape transmitted through the cavity permits optimization of both the cavity lock and dispersion.

stration of high-harmonic generation (HHG) at a 100 MHz repetition rate enabled by a femtosecond enhancement cavity (Jones et al., 2005; Gohle et al., 2005), utilizing the technology discussed in Section 2.2. The process of HHG provides a coherent source of vacuum-ultraviolet to soft x-ray radiation (Corkum, 1993; Lewenstein et al., 1994). Traditionally HHG has only been demonstrated with high-energy, low repetition rate amplified laser systems to provide the peak intensities needed for ionization of a gas target. The small conversion efficiency of the process, combined with the low repetition rate of amplified laser systems, results in low average powers in the XUV generation. Furthermore, the use of these sources as precision spectroscopic tools is limited, as the original laser frequency comb structure is lost in the HHG process. By use of a femtosecond laser coupled to a passive optical cavity, coherent frequency combs in the XUV spectral region are generated via high-harmonics of the laser without any active amplification or decimation of the repetition frequency. Using this technique it's possible to significantly improve the average power conversion efficiency and reduce the system cost and size, while dramatically improving the spectral resolution. Since little of the fundamental pulse energy is converted, a femtosecond enhancement cavity is ideally suited for HHG as the driving pulse is continually recycled after each pass through the gas target. The development of a frequency comb in the XUV and its extreme spectral resolution will likely enable revolutions in precision measurement, quantum control, and ultrafast science, similar to those in the visible and IR regimes.

Figure 26 depicts a simple scheme of intracavity HHG approach. A standard mode-locked femtosecond Ti:sapphire laser with  $f_r$  of 100 MHz, 50-fs pulse duration, and 8 nJ pulse energy is used. The pulse train from the laser passes through a prism-based compressor before impinging upon the passive optical cavity. To couple the pulse train from the mode-locked laser into the cavity, both  $f_o$  and  $f_r$  of the laser are adjusted such that the optical comb components are maxi-

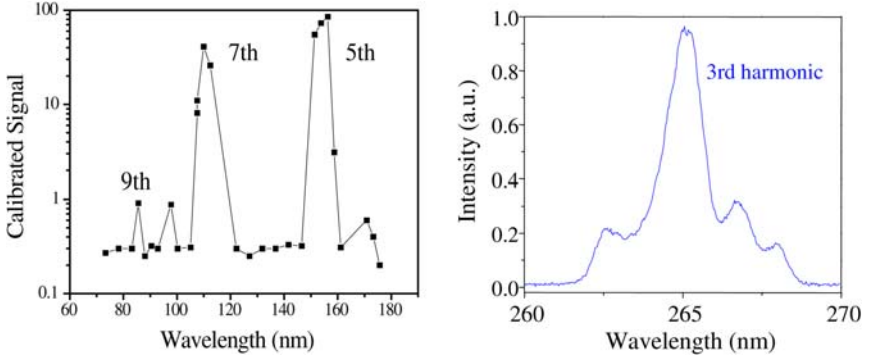


FIG. 27. The output spectrum of the 100-MHz intracavity high harmonic generation.

mally aligned to a set of resonant cavity modes. The enhancement cavity builds up the pulse energy from 8 nJ to 4.8  $\mu$ J, while maintaining the original pulse width and  $f_r$ . The peak intracavity intensity of  $>3 \times 10^{13}$  W/cm<sup>2</sup> is obtained at the intracavity focus. The gas target of Xe atoms is placed slightly after the cavity focus to maximize the HHG light, reducing absorption of the generated optical harmonics. The typical gas pressure at the interaction region is  $>10$  Torr, with  $<1$  mTorr of background pressure for the evacuated chamber where the fs enhancement cavity is located.

To couple the HHG light out of the cavity, a thin sapphire plate is placed at Brewster's angle (for the fundamental comb at near infrared) inside the cavity. This additional optical element, while lowering the cavity finesse only slightly ( $<5\%$ ), requires a negative group-delay-dispersion coated mirror to compensate for the additional material dispersion. The Fresnel reflection coefficient of the intracavity plate rises towards shorter wavelengths in the EUV, with a maximum reflectivity of  $\sim 10\%$  between 30 to 80 nm. The HHG light is then diffracted with a MgF-coated aluminum grating and the resultant spectrum spanning from the 3rd to the 9th harmonics is shown in Fig. 27. With a similar system, the Garching group has observed up to the 15th harmonic (Gohle et al., 2005). The average power of the 3rd harmonic light generated inside the cavity reaches more than 10  $\mu$ W. The single-shot efficiency ( $\approx 10^{-8}$ ) of high harmonic generation using this technique is comparable to traditional amplifier-based systems at similar intensity levels. This demonstrates the dramatic increase in high-harmonic average power that can be accessed using a high repetition rate.

While the use of the intracavity Brewster plate does not impose a serious limitation on the pulse bandwidth under the intracavity dispersion compensation, its nonlinear response does limit the power scalability of the system (Moll et al., 2005). To solve this problem, a novel enhancement cavity configuration that will allow the use of more powerful lasers was designed. One of the focusing cavity

mirrors has a 200  $\mu\text{m}$  hole drilled in the middle to couple out the high-harmonics. By using a higher order cavity mode such as TEM<sub>01</sub>, it is still possible to build up sufficient peak power inside the cavity for HHG, despite the hole in one focusing mirror. The generated VUV comb, however, leaks out of the mirror hole due to the significantly smaller diffraction angles enjoyed by the shorter wavelength light beam (Moll et al., 2006). This cavity geometry will allow a larger buildup power inside the cavity without any intracavity optics. Using this geometry, more powerful laser systems can be explored, such as high energy ( $>25$  nJ pulse energy), chirped-pulse Ti:sapphire oscillators developed by Apolonski and Krausz (Naumov et al., 2005) and power-scalable Yb fiber lasers developed by Hartl of IMRA America, Inc.

High precision measurement of phase/frequency fluctuations in the high-harmonic generation process has also been performed. Two sets of the frequency combs at 266 nm that represent the 3rd harmonic of the fundamental IR comb are brought together for beat detection. One comb is generated by the Xe gas via the HHG process while a second comb is produced by a bulk BBO non-linear crystal. The RF spectrum of the beat note in Fig. 28 shows a clear presence of the comb structure in the UV. The resolution bandwidth-limited 1 Hz beat signal as shown in Fig. 28 demonstrates that the full temporal coherence of the original near-IR comb has been precisely transferred to high harmonics.

### 6.3. FUTURE VUV COMB SPECTROSCOPY

Another motivation for short wavelength spectroscopy is that the simplest atoms, hydrogen and helium, have their first electronic transitions in the VUV spectral range. As previously emphasized, the extremely large peak intensities achievable with femtosecond pulses enables significantly more efficient frequency mixing to generate shorter wavelengths. One of the most interesting future applications of DFCS to extend the realm of coherent spectroscopy of atoms and molecules to shorter wavelengths. Frequency combs also improve the resolution limit past that of current dye laser amplifier techniques used for measuring VUV transitions. One and two-photon cw-laser spectroscopy of the lowest lying electronic transitions in these simplest of atoms have provided direct checks of quantum electrodynamics (Hänsch, 2006; Eikema et al., 1997; de Beauvoir et al., 2000; Bergeson et al., 2000). For example, the Lamb shift of ground state hydrogen and helium has been measured with traditional cw techniques. Another reason for studying these atoms is that the nucleus is simpler in structure and better known than heavy elements. This knowledge of the nucleus allows for better measurements of the Rydberg constant. Currently research is under way in several groups to conduct DFCS of helium to improve measurements of both the ground state Lamb shift

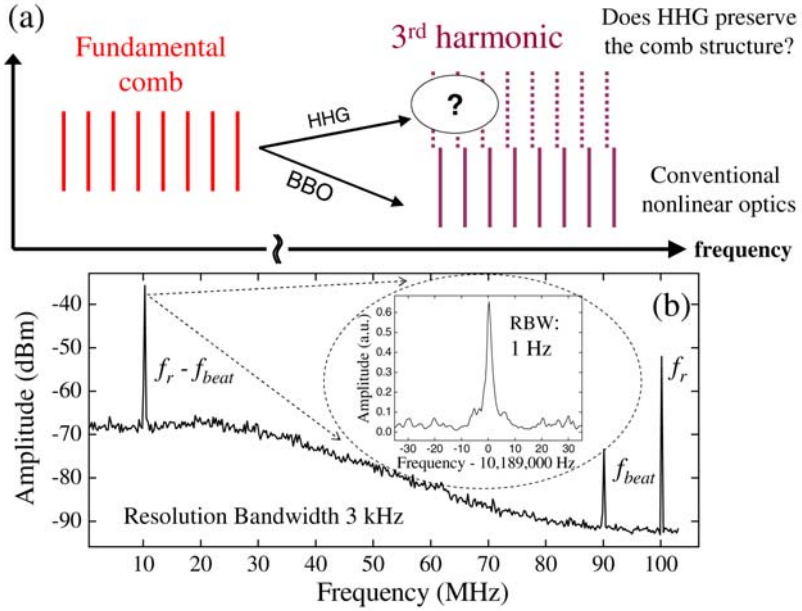


FIG. 28. Coherent heterodyne beat signal is detected between the HHG in Xe gas and bound optical nonlinearities in BBO. These two frequency combs (both at 3rd harmonic) spectrally overlap and provide the optical heterodyne beat signal at an offset radio frequency introduced by an acousto-optical modulator placed in one arm of the interferometer. The two corresponding pulses trains are overlapped in time. The coherent beat signal and repetition frequency detection are shown in (b), demonstrating the HHG comb is phase coherent with respect to its parent comb from the laser, with the coherence limited only by the observation time. The linewidth shown in the inset of (b) is resolution bandwidth (RBW) limited at 1 Hz.

and the Rydberg constant over current cw-laser based measurements. Figure 29 indicates the wavelengths necessary for some one and two-photon transitions of interest in helium. Hydrogen-like, singly charged helium ions is also under current investigation by the group in Garching led by T. Hänsch and T. Udem. One aspect of the regularly spaced mode structure of the comb, important for two-photon transitions, is that if any pair of modes is two-photon resonant then all modes can form a resonant pair. If there is no intermediate state within the bandwidth of the comb, transform limited pulses allow for all of the transition amplitudes driven by the corresponding comb modes to add constructively to the two-photon transition. This is an attractive feature of combs for multi-photon spectroscopy because the entire spectral power contributes to exciting the transition. Another application closely related to spectroscopy at short wavelengths is the laser cooling of atoms at these wavelengths with a frequency comb (Kielipinski, 2006).

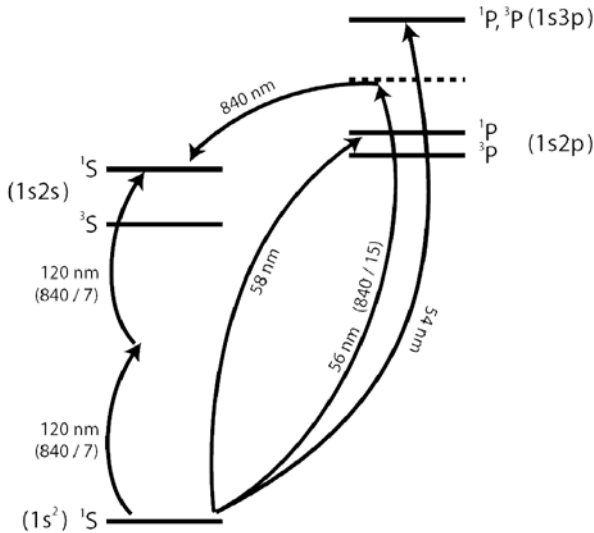


FIG. 29. Several possible interesting excitation paths of helium and corresponding wavelengths based on harmonics of a 840 nm Ti:sapphire laser.

#### 6.4. OPTICAL FREQUENCY SYNTHESIS AND WAVEFORM GENERATION

Femtosecond comb technology has made dramatic advances in time-domain experiments as it has in optical frequency metrology. Stabilization of the “absolute” carrier–envelope phase at a level of tens of milliradians has been demonstrated and maintained over minutes, laying the groundwork for electric field synthesis. The capability of precisely controlling pulse timing and the carrier–envelope phase allows one to manipulate pulses using novel techniques and achieve unprecedented levels of flexibility and precision. For example, comb spectra emitted by independent mode-locked laser sources can now be coherently stitched together (Ye et al., 2002), allowing DFCS to be performed at distinctly different spectral regions while maintaining optical coherence. The related technology development will even allow DFCS to be performed remotely, with optical fiber networks delivering precise frequency comb structure with minimum perturbation (Holman et al., 2004; Hudson et al., 2006).

To establish phase coherence among independent mode-locked lasers, it is necessary to first achieve synchronization among these lasers and reduce the remaining timing jitter below the optical oscillation period (Ma et al., 2001; Shelton et al., 2002a; Schibli et al., 2003). Detecting timing jitter should be carried out at a high harmonic of  $f_r$  to attain much-enhanced detection sensitivity. The second step in achieving phase locking of separate femtosecond lasers requires effective stabilization of the phase difference between the two optical carrier

waves (Shelton et al., 2001, 2002b; Holman et al., 2003b; Bartels et al., 2004b; Kobayashi et al., 2005). Phase locking demands that the spectral combs of individual lasers be maintained exactly coincident in the region of spectral overlap so that the two sets of combs form a continuous and phase-coherent entity. A coherent heterodyne-beat signal between the frequency combs can be used to yield information about the difference in the offset frequencies, which can then be controlled, resulting in two pulse trains with nearly identical phase evolution.

Phase-coherent femtosecond combs have been extended to the mid-infrared spectral region (Foreman et al., 2003, 2005; Zimmermann et al., 2004). Being able to combine the characteristics of two or more pulsed lasers working at different wavelengths provides a flexible approach to coherent control and it is particularly important for difficult to reach spectral regions. Two independent, pulse-synchronized, and phase-locked mode-locked Ti:sapphire lasers can be used in a difference-frequency generation (DFG) experiment to produce phase coherent frequency combs in the mid-IR region, with the wavelength spanning a few to tens of microns. The capability of expanding the spectral coverage of frequency combs while maintain phase coherence is an important ingredient for the goal of optical arbitrary waveform synthesizer. The other important component is precise spectral shaping, including both amplitude and phase. Indeed, an optical arbitrary waveform synthesizer will be the ultimate tool for DFCS, permitting precision spectroscopy and high-resolution quantum control of matter across a vast range of energy scale.

## **7. Concluding Remarks**

Once wide-bandwidth, precisely stabilized optical frequency combs became available in laboratories, direct frequency comb spectroscopy has made rapid progress and found many different applications. Its future impact remains promising for a number of scientific and technological fields, including precision spectroscopy, high-resolution quantum control, arbitrary optical waveform synthesis, long-distance communications, and extreme nonlinear physics. Development of frequency combs at various spectral regions, with the capability of controlling both the time-domain coherence and spectral-domain phase, will no doubt make DFCS an attractive tool to study many atomic, molecular, and condensed matter systems.

## **8. Acknowledgements**

We sincerely thank many of our colleagues and coworkers who have made critical contributions to the work reported in this review. In particular, R.J. Jones led the

initial effort and, along with K.D. Moll, T.R. Schibli, D. Yost, and D. Hudson, carried out a large portion of the femtosecond enhancement cavity work. A. Marian, D. Felinto, and J. Lawall are important contributors to the initial development of broadband DFCS work. A. Bartels, T. Fortier, L. Hollberg, Y. Le Coq, V. Mbele, C. Oates, D. Ortega, and C. Tanner are acknowledged for their invaluable contributions to the Ca and Cs spectroscopy, and the VIPA-based spectrometer. We benefited from useful discussions with E. Eyler, J.L. Hall, S.T. Cundiff, F. Cruz and A. Weiner. Low-loss, low-dispersion, and wide-bandwidth mirrors are provided by R. Lalezari of Advanced Thin Films. We also thank A. Fernandez, A. Apolonski, F. Krausz, I. Hartl, and M. Fermann for providing high energy femtosecond oscillators. Finally, we gratefully acknowledge funding support from NIST, AFOSR, ONR, NSF, and NASA. A. Pe'er thanks the Fulbright foundation for financial support. J.E. Stalnaker gratefully acknowledges the support of the National Research Council. Finally, we thank T. Schibli and T. Fortier for their many useful comments on the manuscript.

## 9. References

- Anderson, D.Z., Frisch, J.C., Masser, C.S. (1984). Mirror reflectometer based on optical cavity decay time. *Appl. Opt.* **23**, 1238–1245.
- Apolonski, A., Poppe, A., Tempea, G., Spielmann, C., Udem, T., Holzwarth, R., Hänsch, T.W., Krausz, F. (2000). Controlling the phase evolution of few-cycle light pulses. *Phys. Rev. Lett.* **85**, 740–743.
- Arissian, L., Diels, J.-C. (2006). Repetition rate spectroscopy of the dark line resonance in Rubidium. *Opt. Comm.* **264**, 169–173.
- Aumiler, D., Ban, T., Skenderović, H., Pichler, G. (2005). Velocity selective optical pumping of Rb hyperfine lines induced by a train of femtosecond pulses. *Phys. Rev. Lett.* **95**, 233001.
- Baklanov, Y.V., Chebotayev, V.P. (1977). Narrow resonances of two-photon absorption of super-narrow pulses in a gas. *Appl. Phys.* **12**, 97–99.
- Balling, P., Maas, D.J., Noordam, L.D. (1994). Interference in climbing a quantum ladder system with frequency-chirped pulses. *Phys. Rev. A* **50**, 4276–4285.
- Ban, T., Aumiler, D., Skenderovic, H., Pichler, G. (2006). Mapping of the optical frequency comb to the atom-velocity comb. *Phys. Rev. A* **73**, 043407-1-10.
- Baltuška, A., Udem, T., Uiberacker, M., Hentschel, M., Goulielmakis, E., Gohle, C., Holzwarth, R., Yakovlev, V.S., Scrinzi, A., Hänsch, T.W., Krausz, F. (2003). Attosecond control of electronic processes by intense light fields. *Nature* **421**, 611–615.
- Bardeen, C.J., Wang, Q., Shank, C.V. (1995). Selective excitation of vibrational wave-packet motion using chirped pulses. *Phys. Rev. Lett.* **75**, 3410–3413.
- Bartels, A., Oates, C.W., Hollberg, L., Diddams, S.A. (2004a). Stabilization of femtosecond laser frequency combs with subhertz residual linewidths. *Opt. Lett.* **29**, 1081–1083.
- Bartels, A., Newbury, N.R., Thomann, I., Hollberg, L., Diddams, S.A. (2004b). Broadband phase-coherent optical frequency synthesis with actively linked Ti:sapphire and Cr:forsterite femtosecond lasers. *Opt. Lett.* **29**, 403–405.
- Bergeson, S.D., Baldwin, K.G.H., Lucatorto, T.B., McIlrath, T.J., Cheng, C.H., Eyler, E.E. (2000). Doppler-free two-photon spectroscopy in the vacuum ultraviolet: Helium  $1^1S$ – $2^1S$  transition. *J. Opt. Soc. Am. B* **17**, 1599–1606.

- Bordé, C.J., Salomon, Ch., Avrillier, S., Van Lerberghe, A., Bréant, Ch., Bassi, D., Scoles, G. (1984). Optical Ramsey fringes with traveling waves. *Phys. Rev. A* **30**, 1836–1848.
- Boyd, M.M., Zelevinsky, T., Ludlow, A.D., Foreman, S.M., Blatt, S., Ido, T., Ye, J. (2006). Optical atomic coherence at the 1-second time scale. *Science* **314**, 1430–1433.
- Brattke, S., Kallmann, U., Hartmann, W.-D. (1998). Coherent dark states of Rubidium 87 in a buffer gas using pulsed laser light. *Eur. Phys. J. D* **3**, 159–161.
- Cao, J., Bardeen, C.J., Wilson, K.R. (1998). Molecular “ $\pi$  pulse” for total inversion of electronic state population. *Phys. Rev. Lett.* **80**, 1406–1409.
- Casperson, L.W. (1998). Few-cycle pulses in two-level media. *Phys. Rev. A* **57**, 609–621.
- Chatel, B., Degert, J., Stock, S., Girard, B. (2003). Competition between sequential and direct paths in a two-photon transition. *Phys. Rev. A* **68**, 041402-1-4.
- Chatel, B., Degert, J., Girard, B. (2004). Role of quadratic and cubic spectral phases in ladder climbing with ultrashort pulses. *Phys. Rev. A* **70**, 053414-1-10.
- Chen, L.-S., Ye, J. (2003). Extensive, high-resolution measurement of hyperfine interactions: Precise investigations of molecular potentials and wave functions. *Chem. Phys. Lett.* **381**, 777–783.
- Chen, L.-S., Cheng, W.Y., Ye, J. (2004). Hyperfine interactions and perturbation effects in the  $B0_u^+$  ( $3\Pi_u$ ) state of  $^{127}\text{I}_2$ . *J. Opt. Soc. Am. B* **21**, 820–832.
- Chen, L.-S., de Jong, W.A., Ye, J. (2005). Characterization of the molecular iodine electronic wave functions and potential energy curves through hyperfine interactions in  $B0_u^+$  ( $3\Pi_u$ ) state. *J. Opt. Soc. Am. B* **22**, 951–961.
- Corkum, P.B. (1993). Plasma perspective on strong-field multiphoton ionization. *Phys. Rev. Lett.* **71**, 1994–1997.
- Couillaud, B., Ducasse, A., Sarger, L., Boscher, D. (1980). High-resolution saturated absorption spectroscopy with coherent trains of short light pulses. *Appl. Phys. Lett.* **36**, 407–409.
- Crosson, E.R., Haar, P., Marcus, G.A., Schwettman, H.A., Paldus, B.A., Spence, T.G., Zare, R.N. (1999). Pulse-stacked cavity ring-down spectroscopy. *Rev. Sci. Instrum.* **70**, 4–10.
- Cruz, F.C., Stowe, M.C., Ye, J. (2006). Tapered semiconductor amplifiers for optical frequency combs in the near infrared. *Opt. Lett.* **31**, 1337–1339.
- Cundiff, S.T., Ye, J. (2003). Colloquium: Femtosecond optical frequency combs. *Rev. Mod. Phys.* **75**, 325–342.
- Cundiff, S.T., Ye, J., Hall, J.L. (2001). Optical frequency synthesis based on mode-locked lasers. *Rev. Sci. Instrum.* **72**, 3749–3771.
- de Beauvoir, B., Schwob, C., Acef, O., Jozefowski, L., Hilico, L., Nez, F., Julien, L., Clairon, A., Biraben, F. (2000). Metrology of the hydrogen and deuterium atoms: Determination of the Rydberg constant and Lamb shifts. *Eur. Phys. J. D* **12**, 61–93.
- Degenhardt, C., Stoehler, H., Lisdat, C., Wilpers, G., Schnatz, H., Lipphardt, B., Nazarova, T., Pottie, P.-E., Sterr, U., Helmcke, J., Riehle, F. (2005). Calcium optical frequency standard with ultracold atoms: Approaching  $10^{-15}$  relative uncertainty. *Phys. Rev. A* **72**, 62111-1-7.
- Delagnes, J.C., Blanchet, V., Bouchene, M.A. (2003). Role of the radiated field in the propagation of an ultra-short chirped pulse. *Opt. Comm.* **227**, 125–131.
- Diddams, S.A., Diels, J.-C., Atherton, B.W. (1998). Differential intracavity phase spectroscopy and its application to a three-level system in samarium. *Phys. Rev. A* **58**, 2252–2264.
- Diddams, S.A., Jones, D.J., Ye, J., Cundiff, S.T., Hall, J.L., Ranka, J.K., Windeler, R.S., Holzwarth, R., Udem, T., Hänsch, T.W. (2000). Direct link between microwave and optical frequencies with a 300 THz femtosecond laser comb. *Phys. Rev. Lett.* **84**, 5102–5105.
- Diddams, S.A., Udem, T., Bergquist, J.C., Curtis, E.A., Drullinger, R.E., Hollberg, L., Itano, W.M., Lee, W.D., Oates, C.W., Vogel, K.R., Wineland, D.J. (2001). An optical clock based on a single trapped  $^{199}\text{Hg}^+$  ion. *Science* **293**, 825–828.
- Diddams, S., Hollberg, L., Mbele, V. (2006). High-resolution spectral fingerprinting with a stabilized femtosecond laser frequency comb. In: *15th International Conference on Ultrafast Phenomena, Technical Digest (CD)*. Optical Society of America. Paper WA3.

- Diddams, S., Hollberg, L., Mbele, V. (2007). Molecular fingerprinting with the resolved modes of a femtosecond laser frequency comb. *Nature* **445**, 627–630.
- Drever, R.W.P., Hall, J.L., Kowalski, F.V., Hough, J., Ford, G.M., Munley, A.J., Ward, H. (1983). Laser phase and frequency stabilization using an optical resonator. *Appl. Phys. B* **31**, 97–105.
- Dudley, J.M., Genty, G., Coen, S. (2006). Supercontinuum generation in photonic crystal fiber. *Rev. Mod. Phys.* **78**, 1135–1184.
- Dudovich, N., Polack, T., Pe'er, A., Silberberg, Y. (2005). Simple route to strong field control. *Phys. Rev. Lett.* **94**, 083002-1-4.
- Eckstein, J.N., Ferguson, A.I., Hänsch, T.W. (1978). High-resolution 2-photon spectroscopy with picosecond light-pulses. *Phys. Rev. Lett.* **40**, 847–850.
- Eikema, K.S.E., Ubachs, W., Vassen, W., Hogervorst, W. (1997). Lamb shift measurement in the  $1S_1$  ground state of Helium. *Phys. Rev. A* **55**, 1866–1884.
- Ell, R., Morgner, U., Kartner, F.X., Fujimoto, J.G., Ippen, E.P., Scheuer, V., Angelow, G., Tschudi, T., Lederer, M.J., Boiko, A., Luther-Davies, B. (2001). Generation of 5-fs pulses and octave-spanning spectra directly from a Ti:sapphire laser. *Opt. Lett.* **26**, 373–375.
- Felinto, D., Acioli, L.H., Vianna, S.S. (2004). Accumulative effects in the coherence of three-level atoms excited by femtosecond-laser frequency combs. *Phys. Rev. A* **70**, 043403-1-10.
- Ferguson, A.I., Eckstein, J.N., Hänsch, T.W. (1979). Polarization spectroscopy with ultrashort light pulses. *Appl. Phys.* **18**, 257–260.
- Foreman, S.M., Jones, D.J., Ye, J. (2003). Flexible and rapidly configurable femtosecond pulse generation in the mid-IR. *Opt. Lett.* **28**, 370–372.
- Foreman, S.M., Marian, A., Ye, J., Petrukhin, E.A., Gubin, M.A., Mücke, O.D., Wong, F.N.C., Ippen, E.P., Kärtner, F.X. (2005). Demonstration of a HeNe/CH<sub>4</sub>-based optical molecular clock. *Opt. Lett.* **30**, 570–572.
- Foreman, S.M., Holman, K.W., Hudson, D.D., Jones, D.J., Ye, J. (2007). Remote transfer of ultrastable frequency references via fiber networks. *Rev. Sci. Instrum.* **78**, 021101-1-25.
- Fortier, T.M., Jones, D.J., Cundiff, S.T. (2003). Phase stabilization of an octave-spanning Ti:sapphire laser. *Opt. Lett.* **28**, 2198–2200.
- Fortier, T.M., Bartels, A., Diddams, S.A. (2006a). Octave-spanning Ti:sapphire laser with a repetition rate >1 GHz for optical frequency measurements and comparisons. *Opt. Lett.* **31**, 1011–1013.
- Fortier, T.M., Le Coq, Y., Stalnaker, J.E., Ortega, D., Diddams, S.A., Oates, C.W., Hollberg, L. (2006b). Kiloherzt-resolution spectroscopy of cold atoms with an optical frequency comb. *Phys. Rev. Lett.* **97**, 163905-1-4.
- Fukuda, Y., Hayashi, J., Kondo, K., Hashi, T. (1981). Synchronized quantum beat spectroscopy using periodic impact excitations with CW mode-locked laser pulses. *Opt. Comm.* **38**, 357–360.
- Garraway, B.M., Suominen, K. (1995). Wave-packet dynamics: new physics and chemistry in femto-time. *Rep. Prog. Phys.* **58**, 365–419.
- Gaubatz, U., Rudecki, P., Schieman, S., Bergmann, K. (1990). Population transfer between molecular vibrational levels by stimulated Raman scattering with partially overlapping laser fields. A new concept and experimental results. *J. Chem. Phys.* **92**, 5363–5376.
- Genkin, G.M. (1998). Rabi frequency and nonlinearity of a two-level atom for an ultrashort optical pulse. *Phys. Rev. A* **58**, 758–760.
- Gerginov, V., Tanner, C.E., Diddams, S., Bartels, A., Hollberg, L. (2004). Optical frequency measurements of  $6s^2S_{1/2} \rightarrow 6p^2P_{3/2}$  transition in a  $^{133}\text{Cs}$  atomic beam using a femtosecond laser frequency comb. *Phys. Rev. A* **70**, 42505-1-8.
- Gerginov, V., Tanner, C.E., Diddams, S.A., Bartels, A., Hollberg, L. (2005). High-resolution spectroscopy with a femtosecond laser frequency comb. *Opt. Lett.* **30**, 1734–1736.
- Gerginov, V., Calkins, K., Tanner, C.E., McFerran, J.J., Diddams, S., Bartels, A., Hollberg, L. (2006). Optical frequency measurements of  $6s^2S_{1/2} \rightarrow 6p^2P_{1/2}(D_1)$  transitions in  $^{133}\text{Cs}$  and their impact on the fine-structure constant. *Phys. Rev. A* **73**, 32504-1-10.

- Gherman, T., Eslami, E., Romanini, D., Kassı, S., Vial, J.-C., Sadeghi, N. (2004). High sensitivity broad-band mode-locked cavity-enhanced absorption spectroscopy: Measurement of  $\text{Ar}^*(^3P_2)$  atom and  $\text{N}_2^+$  ion densities. *J. Phys. D* **37**, 2408–2415.
- Gohle, C., Udem, T., Herrmann, M., Rauschenberger, J., Holzwarth, R., Schuessler, H.A., Krausz, F., Hänsch, T.W. (2005). A frequency comb in the extreme ultraviolet. *Nature* **436**, 234–237.
- Greenland, P.T. (1983). Resonances excited by a train of delta function pulses. *J. Phys. B: At. Mol. Phys.* **16**, 2515–2521.
- Hall, J.L. (2006). Nobel lecture: Defining and measuring optical frequencies. *Rev. Mod. Phys.* **78**, 1279–1295.
- Hall, J.L., Bordé, C.J., Uehara, K. (1976). Direct optical resolution of the recoil effect using saturated absorption spectroscopy. *Phys. Rev. Lett.* **37**, 1339–1342.
- Halzwarth, R., Nevsky, A.Yu., Zimmermann, M., Udem, Th., Hänsch, T.W., Von Zanthier, J., Walther, H., Knight, J.C., Wadsworth, W.J., Russell, P.St.J., Skvortsov, M.N., Bagayev, S.N. (2001). Absolute frequency measurement of iodine lines with a femtosecond optical synthesizer. *Appl. Phys. B* **73**, 269–271.
- Hänsch, T.W. (2006). Nobel lecture: Passion for precision. *Rev. Mod. Phys.* **78**, 1297–1309.
- Hänsch, T.W., Wong, N.C. (1980). Two-photon spectroscopy with an FM laser. *Metrologia* **16**, 101–104.
- Harde, H., Burggraf, H. (1982). Ultrahigh-resolution coherence spectroscopy by means of periodic excitation with picosecond pulses. *Opt. Comm.* **40**, 441–445.
- Heavner, T.P., Jefferts, S.R., Donley, E.A., Shirley, J.H., Parker, T.E. (2005). NIST-F1: Recent evaluations and accuracy improvements. *Metrologia* **42**, 411–422.
- Holman, K.W., Jones, R.J., Marian, A., Cundiff, S.T., Ye, J. (2003a). Intensity-related dynamics of femtosecond frequency combs. *Opt. Lett.* **28**, 851–853.
- Holman, K.W., Jones, D.J., Ye, J., Ippen, E.P. (2003b). Orthogonal control of the frequency comb dynamics of a mode-locked laser diode. *Opt. Lett.* **28**, 2405–2407.
- Holman, K.W., Jones, D.J., Hudson, D.D., Ye, J. (2004). Precise frequency transfer through a fiber network by use of 1.5  $\mu\text{m}$  mode-locked sources. *Opt. Lett.* **29**, 1554–1556.
- Hudson, D.D., Foreman, S.M., Cundiff, S.T., Ye, J. (2006). Synchronization of mode-locked femtosecond lasers through a fiber link. *Opt. Lett.* **31**, 1951–1953.
- Jenkins, F.A., White, H.E. (1976). “Fundamentals of Optics”, 4th edition. McGraw Hill, New York.
- Jonas, D.M. (2003). Two-dimensional femtosecond spectroscopy. *Annual Rev. Phys. Chem.* **54**, 425–463.
- Jones, R.J., Diels, J.-C. (2001). Stabilization of femtosecond lasers for optical frequency metrology and direct optical to radio frequency synthesis. *Phys. Rev. Lett.* **86**, 3288–3291.
- Jones, R.J., Ye, J. (2002). Femtosecond pulse amplification by coherent addition in a passive optical cavity. *Opt. Lett.* **27**, 1848–1850.
- Jones, R.J., Ye, J. (2004). High-repetition-rate coherent femtosecond pulse amplification with an external passive optical cavity. *Opt. Lett.* **29**, 2812–2814.
- Jones, D.J., Diddams, S.A., Ranka, J.K., Stentz, A., Windeler, R.S., Hall, J.L., Cundiff, S.T. (2000). Carrier-envelope phase control of femtosecond mode-locked lasers and direct optical frequency synthesis. *Science* **288**, 635–639.
- Jones, R.J., Thomann, I., Ye, J. (2004). Precision stabilization of femtosecond lasers to high-finesse optical cavities. *Phys. Rev. A* **69**, 051803-1-4.
- Jones, R.J., Moll, K.D., Thorpe, M.J., Ye, J. (2005). Phase-coherent frequency combs in the vacuum ultraviolet via high-harmonic generation inside a femtosecond enhancement cavity. *Phys. Rev. Lett.* **94**, 193201-1-4.
- Kielpinski, D. (2006). Laser cooling of atoms and molecules with ultrafast pulses. *Phys. Rev. A* **73**, 063407-1-6.
- Kobayashi, Y., Yoshitomi, D., Kakehata, M., Takada, H., Torizuka, K. (2005). Long-term optical phase locking between femtosecond Ti:sapphire and Cr:forsterite lasers. *Opt. Lett.* **30**, 2496–2498.

- Lee, K.F., Villeneuve, D.M., Corkum, P.B., Shapiro, E.A. (2004). Phase control of rotational wave packets and quantum information. *Phys. Rev. Lett.* **93**, 233601-1-4.
- Lewenstein, M., Balcou, P., Ivanov, M.Y., Lhuillier, A., Corkum, P.B. (1994). Theory of high-harmonic generation by low-frequency laser fields. *Phys. Rev. A* **49**, 2117–2132.
- Ludlow, A.D., Boyd, M.M., Zelevinsky, T., Foreman, S.M., Blatt, S., Notcutt, M., Ido, T., Ye, J. (2006). Systematic study of the  $^{87}\text{Sr}$  clock transition in an optical lattice. *Phys. Rev. Lett.* **96**, 033003-1-4.
- Ma, L.S., Shelton, R.K., Kapteyn, H.C., Murnane, M.M., Ye, J. (2001). Sub-10-femtosecond active synchronization of two passively mode-locked Ti:sapphire oscillators. *Phys. Rev. A* **64**, 021802-1-4.
- Ma, L.-S., Zucco, M., Picard, S., Robertsson, L., Windeler, R.S. (2003). A new method to determine the absolute mode number of a mode-locked femtosecond-laser comb used for absolute optical frequency measurements. *IEEE Journal of Selected Topics in Quantum Electronics* **9**, 1066–1071.
- Malinovsky, V.S., Krause, J.L. (2001). Efficiency and robustness of coherent population transfer with intense, chirped laser pulses. *Phys. Rev. A* **63**, 043415-1-8.
- Marian, A., Stowe, M.C., Lawall, J.R., Felinto, D., Ye, J. (2004). United time-frequency spectroscopy for dynamics and global structure. *Science* **306**, 2063–2068.
- Marian, A., Stowe, M.C., Felinto, D., Ye, J. (2005). Direct frequency comb measurements of absolute optical frequencies and population transfer dynamics. *Phys. Rev. Lett.* **95**, 023001-1-4.
- Mbele, V., Stalner, J.E., Gerginov, V., Diddams, S.A., Tanner, C.E., Hollberg, L. (in preparation).
- Meshulach, D., Silberberg, Y. (1998). Coherent quantum control of two-photon transitions by a femtosecond laser pulse. *Nature* **396**, 239–242.
- Minoshima, K., Matsumoto, H. (2000). High-accuracy measurement of 240-m distance in an optical tunnel by use of a compact femtosecond laser. *Appl. Opt.* **39**, 5512–5517.
- Mlynek, J., Lange, W., Harde, H., Burggraf, H. (1981). High-resolution coherence spectroscopy using pulse trains. *Phys. Rev. A* **24**, 1099–1102.
- Moll, K.D., Jones, R.J., Ye, J. (2005). Nonlinear dynamics inside femtosecond enhancement cavities. *Opt. Express* **13**, 1672–1678.
- Moll, K.D., Jones, R.J., Ye, J. (2006). Output coupling methods for cavity-based high-harmonic generation. *Opt. Express* **14**, 8189–8197.
- Morgner, U., Ell, R., Metzler, G., Schibli, T.R., Kärtner, F.X., Fujimoto, J.G., Haus, H.A., Ippen, E.P. (2001). Nonlinear optics with phase-controlled pulses in the sub-two-cycle regime. *Phys. Rev. Lett.* **86**, 5462–5465.
- Mücke, O.D., Ell, R., Winter, A., Kim, J.W., Birge, J.R., Matos, L., Kartner, F.X. (2005). Self-referenced 200 MHz octave-spanning Ti:sapphire laser with 50 attosecond carrier-envelope phase jitter. *Opt. Exp.* **13**, 5163–5169.
- Naumov, S., Fernandez, A., Graf, R., Dombi, P., Krausz, F., Apolonski, A. (2005). Approaching the microjoule frontier with femtosecond laser oscillators. *New J. Phys.* **7**, 216.
- Oates, C.W., Curtis, E.A., Hollberg, L. (2000). Improved short-term stability of optical frequency standards: Approaching 1 Hz in 1 s with the Ca standard at 657 nm. *Opt. Lett.* **25**, 1603–1605.
- Oates, C.W., Wilpers, G., Hollberg, L. (2005). Observation of large atomic-recoil-induced asymmetries in cold atom spectroscopy. *Phys. Rev. A* **71**, 23404-1-6.
- O’Keefe, A., Deacon, D.A.G. (1988). Cavity ringdown optical spectrometer for absorption-measurements using pulsed laser sources. *Rev. Sci. Instrum.* **59**, 2544–2551.
- Paulus, G.G., Grasbon, F., Walther, H., Villaresi, P., Nisoli, M., Stagira, S., Priori, E., De Silvestri, S. (2001). Absolute-phase phenomena in photoionization with few-cycle laser pulses. *Nature* **414**, 182–184.
- Pe’er, A., Shapiro, E.A., Stowe, M.C., Shapiro, M., Ye, J. (2007). Precise control of molecular dynamics with a femtosecond frequency comb—A weak field route to strong field coherent control. *Phys. Rev. Lett.* **98**, 113004-1-4.

- Potma, E.O., Jones, D.J., Cheng, J.X., Xie, X.S., Ye, J. (2002). High-sensitivity coherent anti-Stokes Raman scattering microscopy with two tightly synchronized picosecond lasers. *Opt. Lett.* **27**, 1168–1170.
- Potma, E.O., Evans, C., Xie, X.S., Jones, R.J., Ye, J. (2003). High-repetition rate picosecond pulse amplification with an external passive optical cavity. *Opt. Lett.* **28**, 1835–1837.
- Potma, E.O., Xie, X.S., Muntean, L., Preusser, J., Jones, D.J., Ye, J., Leone, S.R., Hinsberg, W.D., Schade, W. (2004). Chemical imaging of photoresists with coherent anti-Stokes Raman scattering (CARS) microscopy. *J. Phys. Chem. B* **108**, 1296–1301.
- Rabitz, H., Vivie-Riedle, R., Motzkus, M., Kompa, K. (2000). Whither the future of controlling quantum phenomena? *Science* **288**, 824–828.
- Ramond, T.M., Diddams, S.A., Hollberg, L. (2002). Phase-coherent link from optical to microwave frequencies by means of the broadband continuum from a 1-GHz Ti:sapphire femtosecond oscillator. *Opt. Lett.* **27**, 1842–1844.
- Ranka, J.K., Windeler, R.S., Stentz, A.J. (2000). Visible continuum generation in air-silica microstructure optical fibers with anomalous dispersion at 800 nm. *Opt. Lett.* **25**, 25–27.
- Reichert, J., Holzwarth, R., Udem, T., Hänsch, T.W. (1999). Measuring the frequency of light with mode-locked lasers. *Opt. Comm.* **172**, 59–68.
- Rice, S.A., Zhao, M. (2000). “Optical Control of Molecular Dynamics”. John Wiley & Sons, New York.
- Salour, M.M., Cohen-Tannoudji, C. (1977). Observation of Ramsey’s interference fringes in the profile of Doppler-free two-photon resonances. *Phys. Rev. Lett.* **38**, 757–760.
- Sautenkov, V.A., Rostovtsev, Y.V., Ye, C.Y., Welch, G.R., Kocharovskaya, O., Scully, M.O. (2005). Electromagnetically induced transparency in rubidium vapor prepared by a comb of short optical pulses. *Phys. Rev. A* **71**, 063804-1-4.
- Scherer, J.J., Paul, J.B., Jiao, H., O’Keefe, A. (2001). Broadband ringdown spectral photography. *Appl. Opt.* **40**, 6725–6732.
- Schibli, T.R., Kim, J., Kuzucu, O., Gopinath, J.T., Tandon, S.N., Petrich, G.S., Kolodziejcki, L.A., Fujimoto, J.G., Ippen, E.P., Kärtner, F.X. (2003). Attosecond active synchronization of passively mode-locked lasers by balanced cross correlation. *Opt. Lett.* **28**, 947–949.
- Schliesser, A., Gohle, C., Udem, T., Hänsch, T.W. (2006). Complete characterization of a broadband high-finesse cavity using an optical frequency comb. *Opt. Exp.* **14**, 5975–5983.
- Shapiro, M., Brumer, P. (1986). Laser control of product quantum state populations in unimolecular reactions. *J. Chem. Phys.* **84**, 4103–4104.
- Shapiro, M., Brumer, P. (2003a). “Principles of the Quantum Control of Molecular Processes”. John Wiley & Sons, Hoboken.
- Shapiro, M., Brumer, P. (2003b). Coherent control of molecular dynamics. *Rep. Prog. Phys.* **66**, 859–942.
- Shelton, R.K., Ma, L.S., Kapteyn, H.C., Murnane, M.M., Hall, J.L., Ye, J. (2001). Phase-coherent optical pulse synthesis from separate femtosecond lasers. *Science* **293**, 1286–1289.
- Shelton, R.K., Foreman, S.M., Ma, L.S., Hall, J.L., Kapteyn, H.C., Murnane, M.M., Notcutt, M., Ye, J. (2002a). Subfemtosecond timing jitter between two independent, actively synchronized, mode-locked lasers. *Opt. Lett.* **27**, 312–314.
- Shelton, R.K., Ma, L.S., Kapteyn, H.C., Murnane, M.M., Hall, J.L., Ye, J. (2002b). Active synchronization and carrier phase locking of two separate mode-locked femtosecond lasers. *J. Mod. Opt.* **49**, 401–409.
- Shirasaki, M. (1996). Large angular dispersion by a virtually imaged phased array and its application to a wavelength demultiplexer. *Opt. Lett.* **21**, 366–368.
- Snadden, M.J., Bell, A.S., Riis, E., Ferguson, A.I. (1996). Two-photon spectroscopy of laser-cooled Rb using a mode-locked laser. *Opt. Comm.* **125**, 70–76.
- Stenger, J., Schnatz, H., Tamm, C., Telle, H.R. (2002). Ultraprecise measurement of optical frequency ratios. *Phys. Rev. Lett.* **88**, 073601-1-4.

- Stowe, M.C., Cruz, F.C., Marian, A., Ye, J. (2006). High resolution atomic coherent control via spectral phase manipulation of an optical frequency comb. *Phys. Rev. Lett.* **96**, 153001-1-4.
- Tannor, D.J., Rice, S.A. (1985). Control of selectivity of chemical reaction via control of wave packet evolution. *J. Chem. Phys.* **83**, 5013–5018.
- Teets, R., Eckstein, J., Hänsch, T.W. (1977). Coherent 2-Photon excitation by multiple light pulses. *Phys. Rev. Lett.* **38**, 760–764.
- Telle, H.R., Steinmeyer, G., Dunlop, A.E., Stenger, J., Sutter, D.H., Keller, U. (1999). Carrier-envelope offset phase control: A novel concept for absolute optical frequency measurement and ultrashort pulse generation. *App. Phys. B* **69**, 327–332.
- Thorpe, M.J., Jones, R.J., Moll, K.D., Ye, J., Lalezari, R. (2005). Precise measurements of optical cavity dispersion and mirror coating properties via femtosecond combs. *Opt. Express* **13**, 882–888.
- Thorpe, M.J., Moll, K.D., Jones, R.J., Safdi, B., Ye, J. (2006). Broadband cavity ringdown spectroscopy for sensitive and rapid molecular detection. *Science* **311**, 1595–1599.
- Thorpe, M.J., Hudson, D.D., Moll, K.D., Lasri, J., Ye, J. (2007). Cavity-ringdown molecular spectroscopy based on an optical frequency comb at 1.45–1.65  $\mu\text{m}$ . *Opt. Lett.* **32**, 307–309.
- Udem, T., Reichert, J., Holzwarth, R., Hänsch, T.W. (1999a). Absolute optical frequency measurement of the Cesium D-1 line with a mode-locked laser. *Phys. Rev. Lett.* **82**, 3568–3571.
- Udem, T., Reichert, J., Holzwarth, R., Hänsch, T.W. (1999b). Accurate measurement of large optical frequency differences with a mode-locked laser. *Opt. Lett.* **24**, 881–883.
- Vidne, Y., Rosenbluh, M., Hänsch, T.W. (2003). Pulse picking by phase-coherent additive pulse generation in an external cavity. *Opt. Lett.* **28**, 2396–2398.
- Vitanov, N.V., Knight, P.L. (1995). Coherent excitation of a two-state system by a train of short pulses. *Phys. Rev. A* **52**, 2245–2261.
- Vitanov, N.V., Fleischhauer, M., Shore, B.W., Bergmann, K. (2001). Coherent manipulation of atoms and molecules by sequential laser pulses. *Adv. At. Mol. Opt. Phys.* **46**, 55–190.
- Wang, S.X., Xiao, S., Weiner, A.M. (2005). Broadband, high spectral resolution 2-D wavelength-parallel polarimeter for dense WDM systems. *Opt. Express* **13**, 9374–9380.
- Weber, K.-H., Sansonetti, C.J. (1987). Accurate energies of  $nS$ ,  $nP$ ,  $nD$ ,  $nF$ , and  $nG$  levels of neutral cesium. *Phys. Rev. A* **35**, 4650–4660.
- Witte, S., Zinkstok, R.T., Ubachs, W., Hogervorst, W., Eikema, K.S.E. (2005). Deep-ultraviolet quantum interference metrology with ultrashort laser pulses. *Science* **307**, 400–403.
- Xiao, S., Weiner, A.M. (2004). 2-D wavelength demultiplexer with potential for  $\geq 1000$  channels in the C-band. *Opt. Express* **12**, 2895–2901.
- Ye, J. (2004). Absolute measurement of a long, arbitrary distance to less than an optical fringe. *Opt. Lett.* **29**, 1153–1155.
- Ye, J., Cundiff, S.T. (Eds.) (2005). *Femtosecond Optical Frequency Comb Technology: Principle, Operation, and Application*. Springer, New York.
- Ye, J., Hall, J.L. (2000). Cavity ringdown heterodyne spectroscopy: High sensitivity with microwatt light power. *Phys. Rev. A* **61**, 061802-1-4(R).
- Ye, J., Ma, L.S., Hall, J.L. (1998). Ultrasensitive detections in atomic and molecular physics – Demonstration in molecular overtone spectroscopy. *J. Opt. Soc. Am. B* **15**, 6–15.
- Ye, J., Hall, J.L., Diddams, S.A. (2000). Precision phase control of an ultrawide-bandwidth femtosecond laser: A network of ultrastable frequency marks across the visible spectrum. *Opt. Lett.* **25**, 1675–1677.
- Ye, J., Ma, L.S., Hall, J.L. (2001). Molecular iodine clock. *Phys. Rev. Lett.* **87**, 270801-1-4.
- Ye, J., Cundiff, S.T., Foreman, S., Fortier, T.M., Hall, J.L., Holman, K.W., Jones, D.J., Jost, J.D., Kapteyn, H.C., Leeuwen, K.A.H.V., Ma, L.-S., Murnane, M.M., Peng, J.L., Shelton, R.K. (2002). Phase-coherent synthesis of optical frequencies and waveforms. *Appl. Phys. B—Lasers & Opt.* **74**, S27–S34.

- Ye, J., Schnatz, H., Hollberg, L.W. (2003). Optical frequency combs: From frequency metrology to optical phase control. *IEEE J. Sel. Top. Quant. Electron.* **9**, 1041–1058.
- Yoon, T.H., Marian, A., Hall, J.L., Ye, J. (2000). Phase-coherent multilevel two-photon transitions in cold Rb atoms: Ultra-high resolution spectroscopy via frequency-stabilized femtosecond laser. *Phys. Rev. A* **63**, 011402-1-4.
- Young, B.C., Cruz, F.C., Itano, W.M., Bergquist, J.C. (1999). Visible lasers with subhertz linewidths. *Phys. Rev. Lett.* **82**, 3799–3802.
- Zewail, A.H. (2000). Femtochemistry: Atomic-scale dynamics of the chemical bond. *J. Phys. Chem. A* **104**, 5660–5694.
- Zimmermann, M., Gohle, C., Holzwarth, R., Udem, T., Hänsch, T.W. (2004). Optical clockwork with an offset-free difference-frequency comb: Accuracy of sum- and difference-frequency generation. *Opt. Lett.* **29**, 310–312.
- Zinkstok, R.Th., Witte, S., Ubachs, W., Hogervorst, W., Eikema, K.S.E. (2006). Frequency comb laser spectroscopy in the vacuum-ultraviolet region. *Phys. Rev. A* **73**, 061801-1-4.
- Ziolkowski, R.W., Arnold, J.M., Gogny, D.M. (1995). Ultrafast pulse interactions with two-level atoms. *Phys. Rev. A* **52**, 3082–3094.